Supplementary Information (SI) for ChemComm.

Supporting Information

Stabilisation and functional enhancement of a metal-organic framework purinate-glass composite

Yujun Rong,[a†] Ashleigh M. Chester,[a†] Bethan Turner,[b] Georgina P. Robertson,[a,c] Ayano Kono,[a] Philip A. Chater,[c] Lauren N. McHugh,[b] David A. Keen,[d] Thomas D. Bennett[a,e] and Celia Castillo-Blas*[a,‡]

[a] Department of Materials Science and Metallurgy, University of Cambridge, Cambridge, CB3 0FS, UK.

[b] Department of Chemistry, University of Liverpool, Crown Street, Liverpool L69 7ZD, UK.

[c] Diamond Light Source Ltd, Diamond House, Oxfordshire, OX11 0DE, UK.

[d] ISIS Facility, Rutherford Appleton Laboratory, Harwell Campus, Didcot, Oxfordshire OX11 0QX, UK

[e] School of Physical and Chemical Sciences, University of Canterbury, Private Bag 4800, Christchurch 8140, New Zealand.

E-mail: castillo@icmm.csic.es

† Both authors contributed equally.

‡ Present address: Materials Science Institute of Madrid – Spanish National Research Council (ICMM-CSIC), C/Sor Juana Inés de la Cruz 3, Madrid, 28049, Spain.

Table of contents

1. Materials and Methods

Materials. Imidazole (≥99.5%), D_2O (35 wt% DCl) and purine (98%) were purchased from Sigma Aldrich. Dimethyl sulfoxide (DMSO)-d_6 (99.8 atom% D, contains 0.03% (v/v) tetramethylsilane (TMS)) was purchased from VWR. Zinc nitrate hexahydrate (98%) was purchased from Alfa Aesar. N,N-Dimethylformamide (DMF) (99.5%), dichloromethane stabilised with amylene (DCM) (99.8%) and terephthalic acid (≥ 98%) were purchased from Fischer Scientific. Zirconium chloride (98%) was purchased from Acros Organics. Phosphate buffer saline solution (PBS, pH 7.4, concentration 1X, which has a concentration of 137 mM NaCl, 2.7 mM KCl, 10 mM Na_2HPO_4, and 1.8 mM KH_2PO_4) was purchased from Fisher Scientific. Methylene blue (MB) hydrate (≥ 97.0%) was purchased from Sigma Aldrich. All materials were used without further purification.

Synthesis of ZIF-UC-7. Following the synthetic procedure described in the literature,[19] a mixture of zinc nitrate hexahydrate (1.515 g, 5.09 mmol), imidazole (7.350 g, 108 mmol) and purine (1.441 g, 12.0 mmol) were dissolved in 75 mL of dimethylformamide (DMF) to give an orange/brown solution in a screw-top jar. The solution was heated to 130 °C and held for 48 hours in an oven. It was then left to cool to room temperature naturally. The resulting yellow-coloured crystals were isolated by vacuum filtration and washed with fresh DMF. The crystals were then soaked in 5 mL of DCM for 24 hours for solvent exchange. The crystals were again isolated by vacuum filtration before being activated under vacuum at 130 °C for three hours. ZIF-UC-7 powder was prepared by ball milling with two 5 mm diameter balls at 20 Hz for 5 minutes using a Retsch MM400 mixer mill.

Synthesis of UiO-66. A mixture of zirconium chloride (0.945 g, 4.06 mmol), terephthalic acid (1.34 g, 8.07 mmol) and hydrochloric acid (0.715 mL) in 24.5 mL of DMF was placed into a 50 mL Teflon vessel PARR autoclave. The mixture was heated at 180 °C for 24 hours in an oven. After cooling, the white solid was collected *via* centrifugation (4000 rpm for five minutes), washed twice with DMF (2 x 20 mL) and solvent exchanged with methanol overnight. The powder was then activated under vacuum at 250 °C overnight, then at 300 °C for three hours.[20]

Glass Formation of ZIF-UC-7. The a_gZIF-UC-7 was synthesised by heating ZIF-UC-7 under an argon flow (100 µL/min) to 350°C at a ramp rate of 10 °C min^{-1} in a TA instruments Q-650 series differential scanning calorimeter. ZIF-UC-7 was held at 350°C for one minute before cooling to 30 °C at 10 °C min^{-1}.

Composite Synthesis. A physical mixture of 99.5 mg of a_gZIF-UC-7 and 99.7 mg of UiO-66 (denoted as (UiO-66) a_gZIF-UC-7)(50/50)) was ball milled using 2 x 5 mm diameter balls at 20 Hz for five minutes using a Retsch MM400 mixer mill . 150 mg of the physical mixture were pressed into a 13 mm pellet dye under a force of 1 tonne (0.074 GPa) for one minute. The pellet was clamped between two glass slides before annealing in a vacuum oven at 300 °C for 10 minutes and cooled to room temperature under vacuum. The method used was based on the low temperature route reported by Li *et al* using pre-prepared a_gZIF-UC-7.

Powder X-Ray Diffraction (PXRD) analysis. Room temperature PXRD data (2θ = 2° to 50°) were collected with a Bruker D8 ADVANCE diffractometer equipped with a LynxEye position-sensitive detector in Bragg–Brentano parafocusing geometry, using Cu Kα radiation (λ = 1.5418 Å). PowDLL was used to convert the .raw data files into .xy format. Pawley refinements were performed in a 2θ = 2° to 50° range, unless specified otherwise in the Figure captions, using TOPAS-Academic Version 6.[1]

Thermalgravimetric analysis (TGA). TGA data were collected with a TA Instruments SDT-Q650 using alumina pans (90 µL). The experiments were conducted under a flowing argon atmosphere at heating rates of 10 °C min^{-1}. All data were analysed using the TA Instruments Universal Analysis software. The starting temperatures of weight changes were determined from the first derivative of the weight (%) trace as a function of temperature.

Differential Scanning Calorimetry (DSC). Data were collected with a Netzsch DSC 214 Polyma Instrument. The experiments were conducted under an argon atmosphere at heating rates of 10 °C min^{-1}. Sealed aluminium pans (30 µL) with a hole punctured in the lid were used to prevent pressure build-up. Background corrections were performed using the same heating cycle on an empty aluminium reference pan. All data were analysed using the Netzsch Proteus® software package. Melting point T_m was taken as the offset (the endpoint) of the melting endotherm. Glass transition temperature T_g was taken as the mid-point of the change in gradient of the heat flow of the DSC upscans.

^{1}H Nuclear Magnetic Resonance (NMR) Spectroscopy. ^{1}H NMR spectra were recorded at ambient temperature using a Bruker AVIII 500 MHz Spectrometer with a dual ^{13}C/^{1}H (DCH) cryoprobe at the Department of Chemistry, University of Cambridge. Crystalline ZIF-UC-7 and a_gZIF-UC-7 samples were dissolved in a mixture of DCl (35%)/D_2O and DMSO-d_6 in a 1:5 ratio. Tetramethylsilane (TMS) was used as a reference. Data processing was performed using the Mestronova software package.

CHN microanalysis. CHN microanalysis experiments were performed using a CE440 Elemental Analyser, EAI Exeter Analytical Inc at the Department of Chemistry, University of Cambridge. Approximately 1-2 mg of sample was used for each measurement.

ICP-OES Analysis. 5 mg of the solid samples were digested using 1 mL of hydrogen peroxide (30% v:v) and 2 mL concentrated sulfuric acid (98%) for 16 hours. Once the solution is clear it is diluted to 15 mL. Analyses were carried out using an ICP-OES AVIO 220 Max, Perking Elmer with axial mode, and operating with wavelength values of 343.823, 206.200 and 213.617 nm for the ZrP20ppm and Zn10ppm methods and 213.617 nm for P200 method. PBS pristine and PBS supernatant after the composite immersion after 24 hours were also analysed (20 mL).

Optical microscopy. Optical images of all samples were obtained using A Leica MZ95 microscope and a Optika C-B10 CMOS with a resolution of 10 megapixels camera. Additional images were obtained with a TOMLOV-DM-9 optical microscope.

Scanning Electron Microscopy (SEM). SEM images were collected with a high-resolution scanning electron microscope FEI Nova Nano SEM 450 at an accelerating voltage of 15 kV for images and EDS mapping. Samples were prepared by dispersing samples onto double-sided adhesive conductive carbon tape on a flat aluminium sample holder and then coated with a gold layer of 15 nm using an Emtech K575 sputter coater. Additional FE-SEM images, EDX analyses and mapping analyses were collected using a FEI Nova NanoSEM 230 microscope with a Schottky field-emission gun operating at 5 KeV for images and 20 KeV for EDX and mapping analyses.

Fourier-transform infrared spectroscopy (FTIR). FTIR spectra were collected with a Brucker Tensor 27 FT-IR Spectrometer using about 5 mg of each sample. Background scans were conducted between each sample scan and the resolution of the scans was 1 cm^{-1}.

Pair distribution function (PDF) analysis. Samples were ground and added to kapton capillaries with inner diameters of 1 mm. Samples were packed to variable heights (~5-8 cm) and sealed with plasticine. Total scattering data for PDF analysis were collected at the I15-1 beamline at the Diamond Light Source, UK (Experiment reference CY31401-1, λ = 0.161669 Å, 76.69 keV). Empty instrument (background) and empty capillary scans were run for all samples.

Raw data were processed using GudrunX in a $0.3 < Q < 20$ $Å^{-1}$ range to correct for background, container, multiple and Compton scattering.[2] Fourier transformation of the processed total scattering data yielded real space pair distribution function, $G(r)$. The $D(r)$ form was used to accentuate high r correlations.[3,4]

Gas sorption. Gas uptake measurements and adsorption analysis of CO_2 up to 0.032 p/p° at 273 K were performed on a Micrometric 3-Flex 3500 Gas Sorption Analyser. Samples of *ca.* 90 mg were degassed *in situ* with nitrogen by heating to 383 K at a rate of 10 K per minute under vacuum for 16 hours. Adsorption and desorption Isotherms were produced, providing values for the maximum uptake and trends in adsorption/desorption. Analysis was performed with Micromeretics Flex Version 6.02 software. The gas uptake measurements and adsorption analysis of N_2 up to 1 p/p° at 77 K were performed on a Micrometric 3-Flex 3500 Gas Sorption Analyser. Samples of *ca.* 90 mg were degassed *in situ* with nitrogen by heating to 373 K at a rate of 10 K per minute under vacuum for 15 hours. Analysis was performed with Micromeretics Flex Version 6.02 software.

Methylene blue uptake and release analysis. Methylene blue (MB) uptake analysis was performed by immersing 5 mg of each sample in 10 mL of 5 ppm MB solution in a sealed glass vial with continuous stirring. The MB solution was prepared by dissolving MB powder in phosphate buffer saline (PBS) solution and PBS was used as a blank. UV-VIS spectrum of the solution was collected after 0.5 h, 1 h, 2 h, 4 h, 6 h, 8 h, 16 h, 24 h, 48 h and 72 h. UV-VIS of all samples were recorded using an Agilent UV-VIS spectrophotometer in a range of 200-800 nm and analysis were performed by fixing the maximum at 664 nm. All measurements were triplicated.

PBS stability tests. PBS stability tests were performed by immersing 5 mg of samples in 10 mL of PBS in a plastic bottle with a lid and mixing with a magnetic stirrer. The pH values (4-6 measurements) for each sample were determined at various time points (1, 2, 3, 6 and 8 days) using a Hanna instruments 2212 pH meter, calibrated using standard pH buffer solutions (pH 4.01 and 7.01). pH values of the solution were collected after 15 mins, 30 mins, 45 mins, 60 mins, 90 mins, 2 h, 3 h, 4 h, 5 h, 24 h, 30 h, 48 h, 72 h, and 160 h.

2. Starting materials characterisation

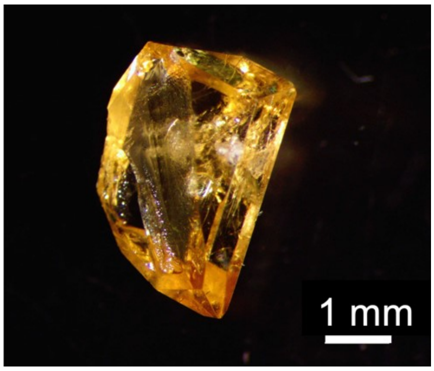

Figure S1. Optical microscope image of ZIF-UC-7 single crystal. Scale bar added using ImageJ 1.52.

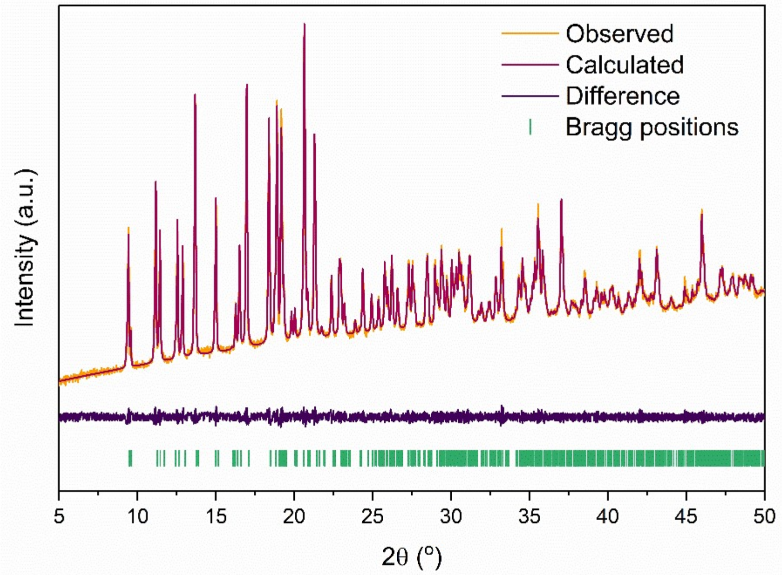

Figure S2. Pawley refinement of powder X-ray diffraction data of ZIF-UC-7, space group *Pbca*, refinement was carried out in a 2θ = 5-50° range. Experimental/observed data (orange line) calculated (red line) and difference plot [(I_{obs}–I_{calc})] (purple line) are shown. Initial parameters were obtained from the crystal structure of ZIF-UC-7, a = 15.1336(5) Å, b = 15.4532(5) Å, c = 8.4151(6) Å.[5] The zero point error (°) was also refined (0.02(10)). The difference curve is offset on the y axis for clarity.

Table S1. Refined values and literature values of ZIF-UC-7 and UiO-66 lattice parameters.

Sample	Lattice parameter	Refined value (Å)	Literature value (Å)	R_{wp}	R_p
ZIF-UC-7	***a***	15.361(2)	15.1336(5)	7.35%	5.34%
	b	15.494(2)	15.4532(5)		
	c	18.526(3)	18.4151(6)		

Table S2. CHN microanalysis of ZIF-UC-7 and *a*$_g$ZIF-UC-7 and comparison with the calculated formula.

Sample	% Found			%Calculated			Formula
	wt% C	wt% H	wt% N	wt% C	wt% H	wt% N	
ZIF-UC-7	37.35	3.34	28.16	39.94	3.77	29.11	[Zn(pur)$_{0.46}$(Im)$_{1.54}$]0.5·DMF
a$_g$ZIF-UC-7	36.14	2.70	30.03	37.28	2.68	31.05	[Zn(pur)$_{0.46}$(Im)$_{1.54}$]

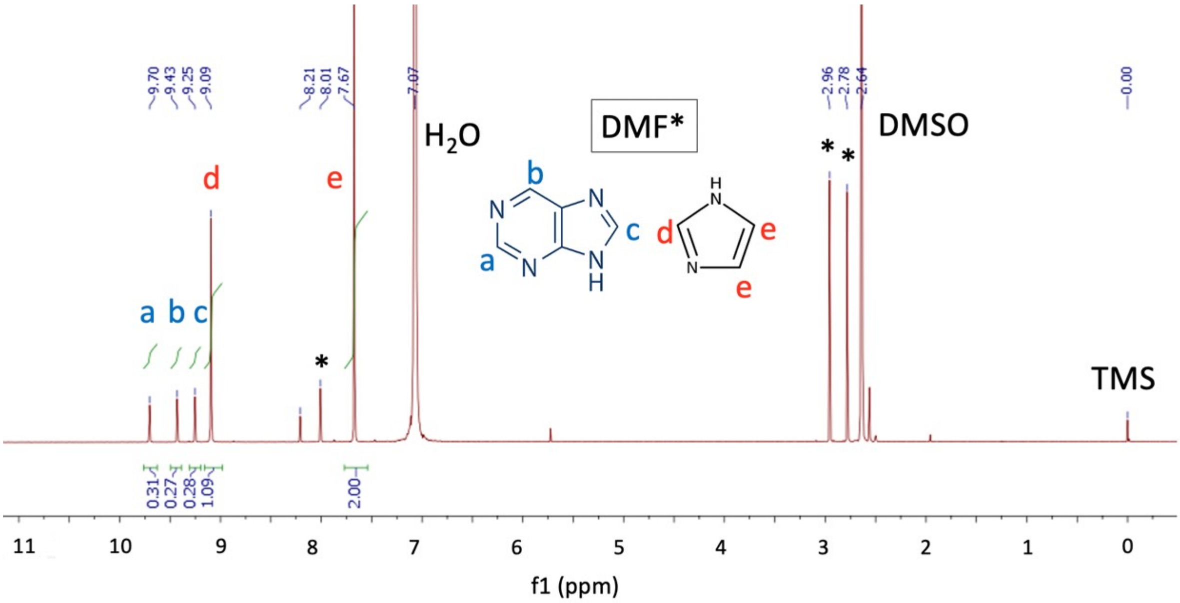

Figure S3. ^{1}H nuclear magnetic resonance (NMR) spectrum of ZIF-UC-7. δ_H (500 MHz; DCl (35%)/D_2O:DMSO-d$_6$ (1:5); Me_4Si) 9.70 (1H, s, H$_a$), 9.43 (1H, s, H$_b$), 9.25 (1H, s, H$_c$), 9.09 (1H, s, H$_d$), 8.01 (DMF), 7.67 (2H, s, H$_e$), 7.07 (H_2O/HCl), 2.96, 2.78 (DMF), 2.64 (DMSO), 0.00 (TMS).

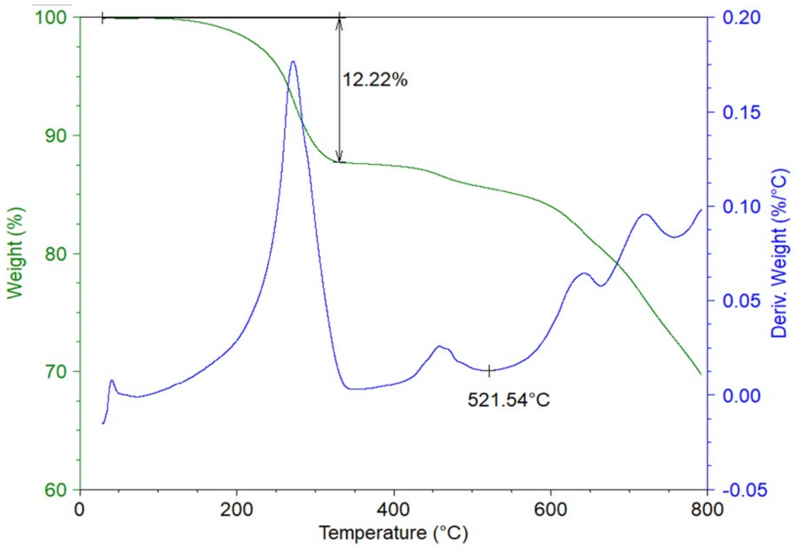

Figure S4. Thermogravimetric analysis of crystalline ZIF-UC-7 heated at 10 °C min^{-1} to 800 °C under argon. Weight (%) curve shown in green and derivative weight (%/°C) shown in blue. Weight loss at 340 °C (~12%) and 520 °C correspond to dimethylformamide and partial decomposition of purinate linker respectively.

DSC analysis was used to assess the T_m and T_g of ZIF-UC-7 and a_gZIF-UC-7. Pre-annealing at 275 °C before DSC measurement was performed on ZIF-UC-7 to release the entrapped DMF from the synthesis, which would obscure DSC features (**Fig. S5**). The first DSC upscan of crystalline ZIF-UC-7 showed a melting endotherm (T_m) of 336.7 °C. Glass transition behaviour was observed in the second upscan (T_g = 273.1 °C), which confirmed that a_gZIF-UC-7 was successfully formed by melt-quenching.

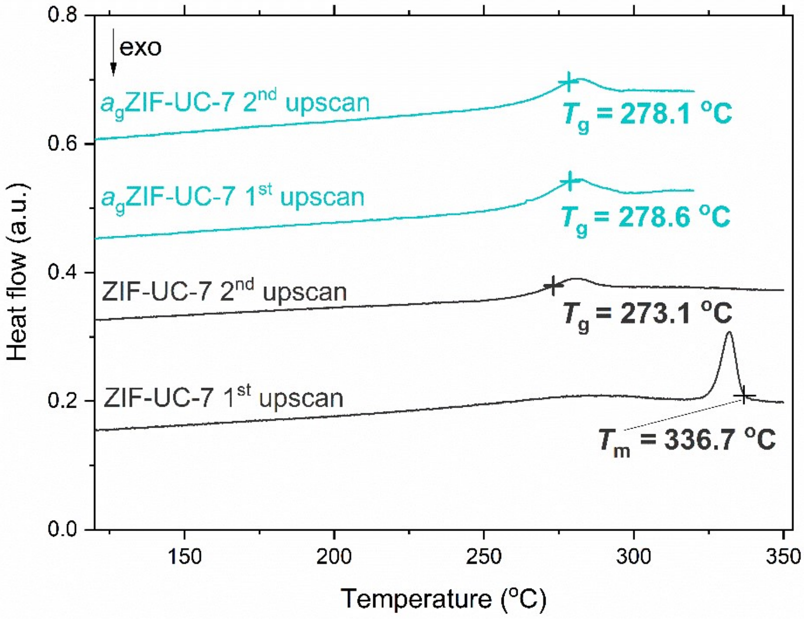

Figure S5. Differential scanning calorimetry (DSC) of crystalline ZIF-UC-7 and a_gZIF-UC-7, showing first and second upscans. ZIF-UC-7 was pre-annealed at 275 °C *in situ*, heated to 400 °C, cooled to 30 °C and then heated to 400 °C. a_gZIF-UC-7 was heated to 350 °C (first upscan), cooled to 30 °C and then heated again to 350 °C (second upscan).

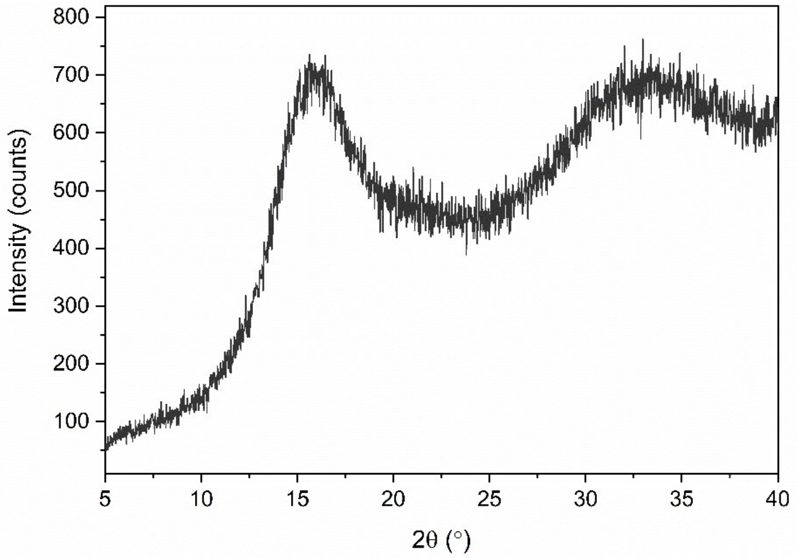

Figure S6. Powder X-ray diffraction pattern of a_gZIF-UC-7.

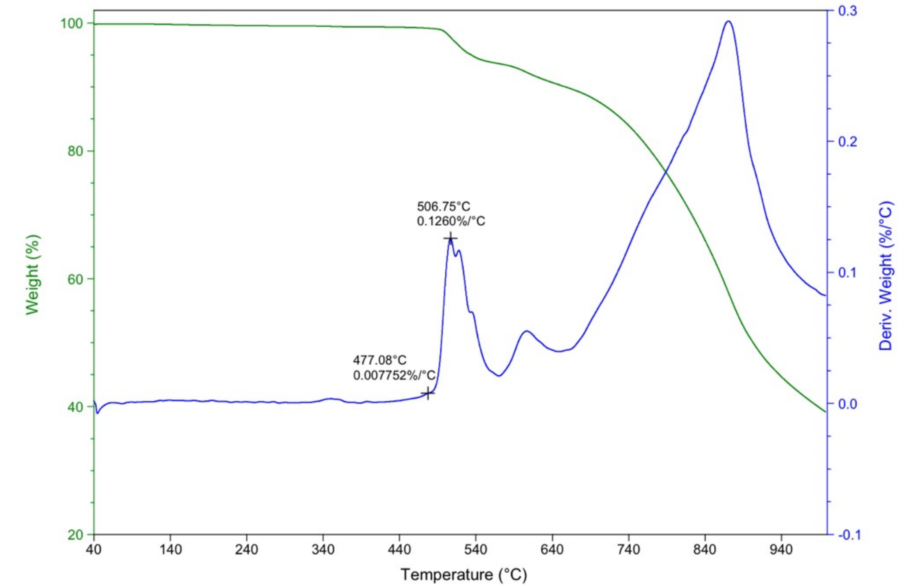

Figure S7. Thermogravimetric analysis of a_gZIF-UC-7 heated at 10 °C min^{-1} to 800 °C under argon. Weight (%) curve shown in green and derivative weight (%/°C) shown in blue.

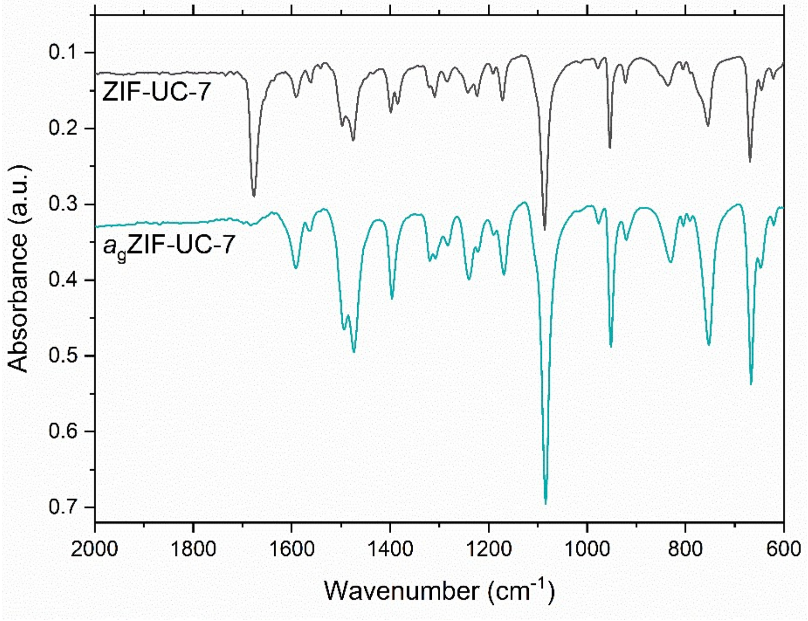

Figure S8. Fourier-transform Infrared spectroscopy of ZIF-UC-7 (black) and a_gZIF-UC-7 (green). FTIR confirms the structural integrity of ZIF-UC-7 was maintained post glass formation. The band at ~1700 cm^{-1} in ZIF-UC-7 is absent in a_gZIF-UC-7, showing that the entrapped DMF in ZIF-UC-7's pores was removed successfully post melt-quenching.

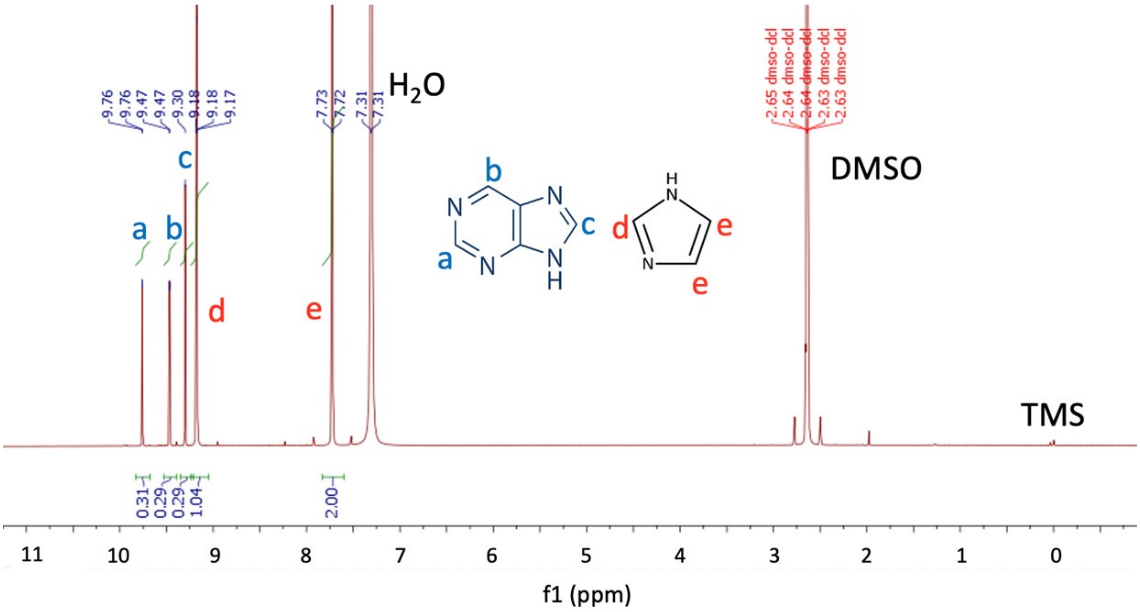

Figure S9. ^{1}H nuclear magnetic resonance (NMR) spectrum of a_gZIF-UC-7. δ_H (500 MHz; DCl(35%)/D_2O:DMSO-d_6 (1:5); Me_4Si) 9.76 (1H, s, H_a), 9.47 (1H, s, H_b), 9.30 (1H, s, H_c), 9.18 (1H, s, H_d), 7.73 (2H, s, H_e), 7.31 (H_2O/HCl), 2.64 (DMSO), 0.00 (TMS).

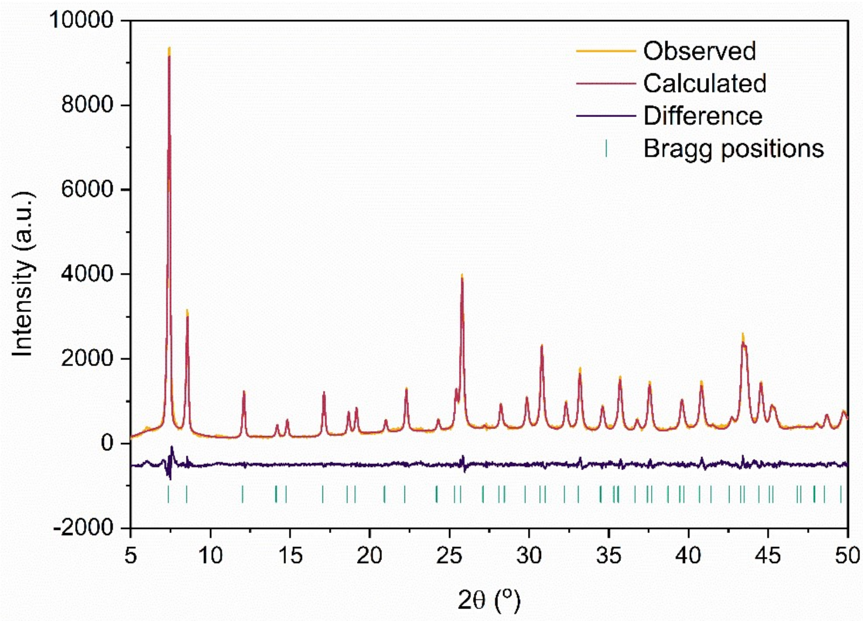

Figure S10. Pawley refinement of powder X-ray diffraction data of UiO-66, space group *Fm-3m*, data were refined between 2θ = 5-50°. Experimental/observed data (orange line), calculated (red line), difference plot [(I_{obs}–I_{calc})] (purple line) and Bragg positions (green) are shown. Initial lattice parameters were obtained from the crystal structure of UiO-66, *a* = 20.768 Å.[6] The difference curve is offset on the y axis for clarity. Zero-point error was also refined, 0.04(20).

Table S3. Refined values and literature values of UiO-66 lattice parameter.

Sample	Cell length/ Å	Refined value	Literature value	R_{wp}
UiO-66	***a***	20.766(7)	20.768	11.7

TGA on UiO-66 shows a T_d of ~521°C. Initial weight loss of ~5.4% corresponds to loss of water, weight loss of ~2.5% above ~177 °C likely corresponds to loss of DMF solvent molecules from the synthesis.

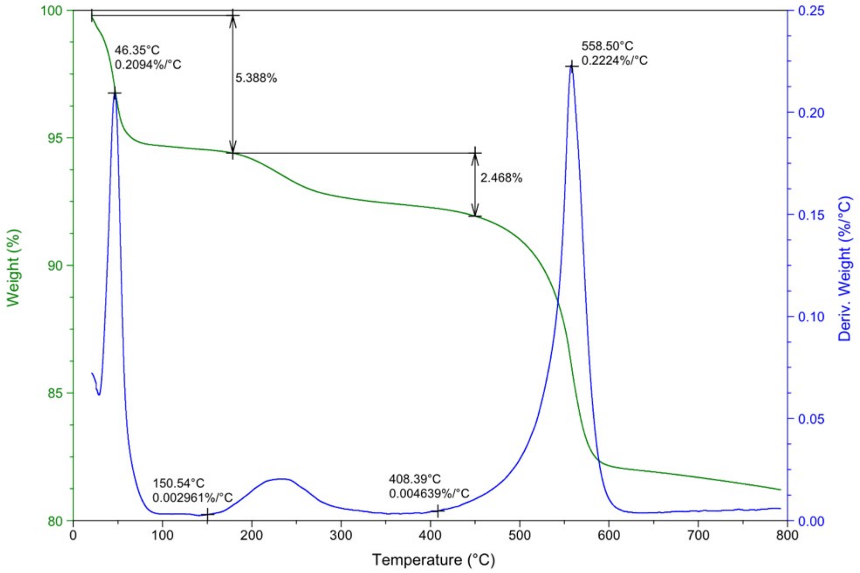

Figure S11. TGA of activated UiO-66, showing a T_d of ~521°C.

3. Selecting the working conditions

Selecting the T_w was an interplay between minimising decomposition of UiO-66 and heating to a temperature exceeding the T_g of a_gZIF-UC-7 (T_g = 278 °C) (**Figure S12**). Negligible decomposition of UiO-66 is observed up to 350 °C, giving a potential working range of 278-350 °C.

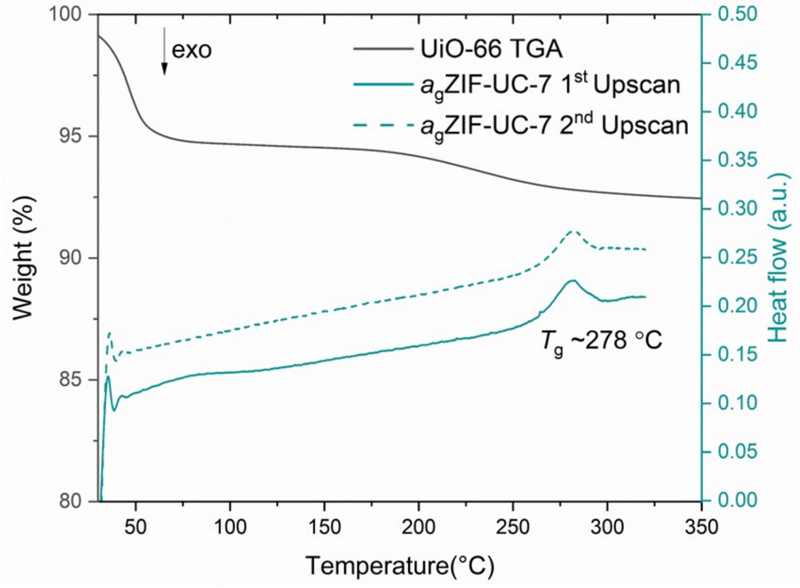

Figure S12. TGA of UiO-66 and 1st and 2nd DSC upscans of a_gZIF-UC-7.

Activated UiO-66 was subjected to different temperature and pressure working conditions (**Figure S13**). UiO-66 powder was pelletised under two different pressures, 0.074 GPa and 0.22 GPa and temperatures (300 and 330 °C). PXRD analysis revealed that pelletisation at 0.22 GPa decreased the intensity of the UiO-66 Bragg peaks, with a recovery in peak height post heating at both temperatures. However, the overall reduction in peak height of the 0.22 GPa 330 °C sample suggested a lower T_w was more suitable and so 300 °C was selected. Additionally, a lower pressure (0.074 GPa) was selected to minimise Bragg peak height loss of UiO-66 during composite formation.

Importantly, the selected annealing temperature was above the T_g of a_gZIF-UC-7, which allowed the glass to enter its liquid state and form a cohesive composite. The time selected was a compromise between facilitating flow of the glass around the MOF particles and the decreased Bragg peak height observed in the UiO-66 controls.

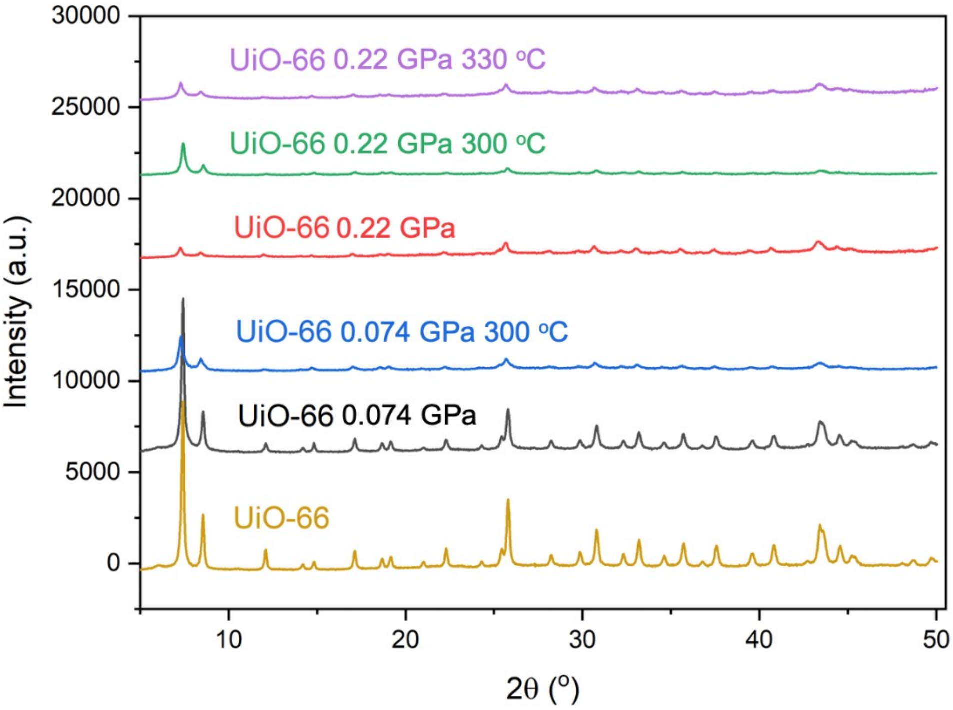

Figure S13. PXRD of UiO-66 pelletised at 1 tonne (0.074 GPa), 3 tonnes (0.22 GPa), annealed in a vacuum oven at 300 and 330 °C.

4. Physical mixture and composite characterisation

4.1 PXRD analysis and FTIR

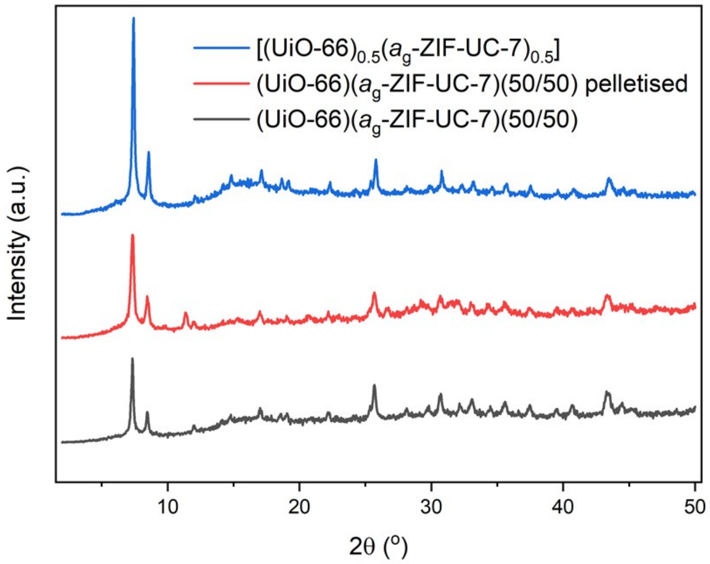

Figure S14. Comparison of the PXRD of the (UiO-66)(a_gZIF-UC-7)(50/50) physical mixture, pelletised (UiO-66)(a_gZIF-UC-7)(50/50) physical mixture and the composite [(UiO-66)$_{0.5}$(agZIF-UC-7)$_{0.5}$].

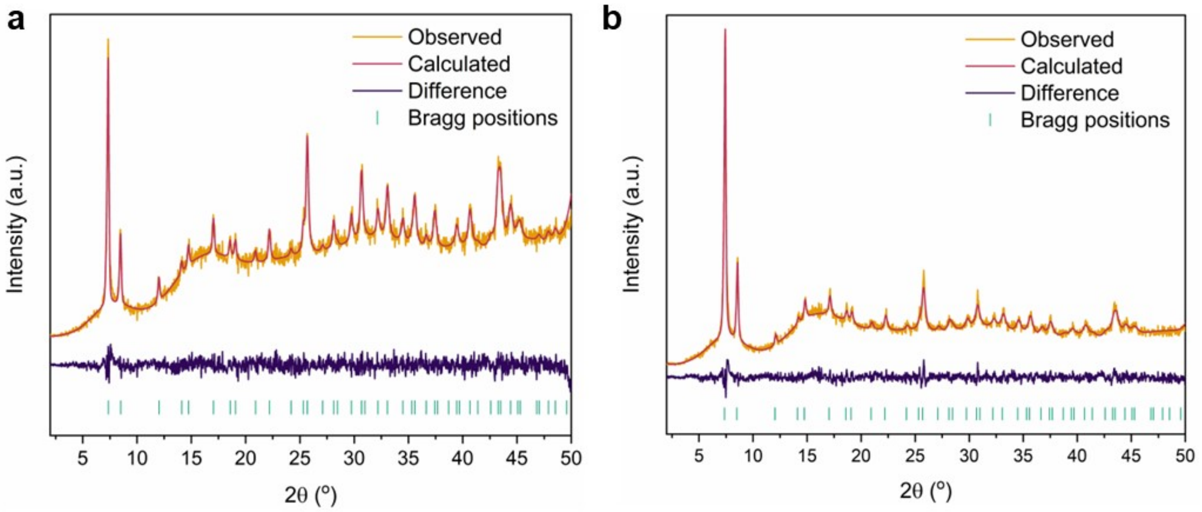

Figure S15. Pawley refinement of powder X-ray diffraction data of **a.** (UiO-66)(a_gZIF-UC-7)(50/50) physical mixture and **b.** [(UiO-66)$_{0.5}$(a_gZIF-UC-7)$_{0.5}$] composite, refined against the crystal structure of UiO-66 (space group *Fm-3m*). Experimental/observed data (orange line), calculated (red line) and difference plot [(I_{obs}–I_{calc})] (purple line) are shown. The difference curve is offset on the y axis for clarity.

Table S4. Pawley refined lattice parameters of the physical mixture and composite.

Sample	Refined lattice parameter *a* (Å)	Literature value (Å)	R_{wp}	R_p
(UiO-66)(a_gZIF-UC-7)(50/50)	20.8(02)	20.768	6.28%	4.59
[(UiO-66)$_{0.5}$(a_gZIF-UC-7)$_{0.5}$]	20.78(3)	20.768	7.66%	5.9

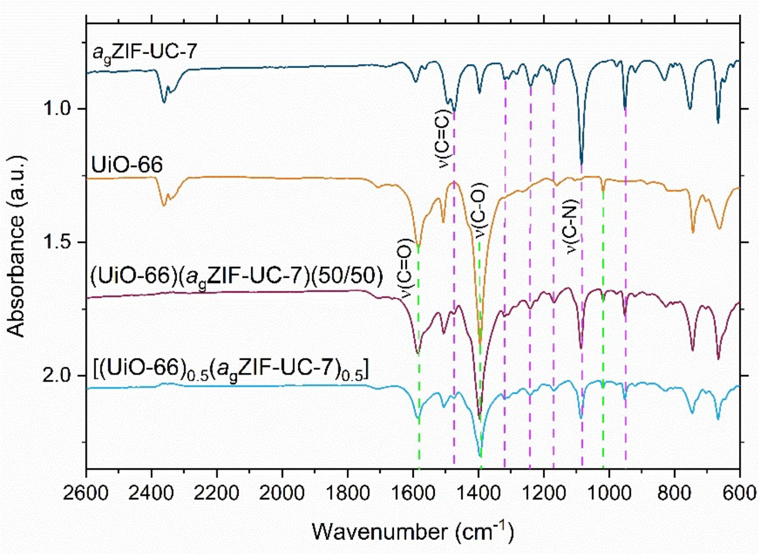

Figure S16. FTIR spectra of a_gZIF-UC-7, UiO-66, (UiO-66)(a_gZIF-UC-7)(50/50) physical mixture and [(UiO-66)$_{0.5}$(a_gZIF-UC-7)$_{0.5}$].

4.2 Compositional analysis

Table S5. CHN microanalysis of UiO-66 and [(UiO-66)$_{0.5}$(a_gZIF-UC-7)$_{0.5}$].

Sample	C wt%	H wt%	N wt%	Molar formula	Chemical formula
UiO-66 theoretical	35.3	1.73	0	NA	$Zr_6O_4(OH)_4(C_8H_4O_4)_6$
UiO-66 experimental	29.34	2.16	0.80	NA	
(UiO-66)(a_gZIF-UC-7)(50/50) theoretical	38.17	2.34	16.49	1:7.43	$Zr_6Zn_{7.43}C_{100}H_{73}N_{37}O_{20}$
(UiO-66)(a_gZIF-UC-7)(50/50) found	37.89	3	17.7	1:7.43	
[(UiO-66)$_{0.5}$(a_gZIF-UC-7)$_{0.5}$] theoretical	38.17	2.34	16.49	1:7.43	$Zr_6Zn_{7.43}C_{100}H_{73}N_{37}O_{20}$
[(UiO-66)$_{0.5}$(a_gZIF-UC-7)$_{0.5}$] found	37.53	2.82	16.65	1:7.43	

The weight percentage of Zn in [(UiO-66)$_{0.5}$(a_gZIF-UC-7)$_{0.5}$] was higher than expected, indicating a higher amount than 50 wt% of a_gZIF-UC-7 in the composite.

Table S6. ICP microanalysis of (UiO-66)(a_gZIF-UC-7)(50/50)and [(UiO-66)$_{0.5}$(a_gZIF-UC-7)$_{0.5}$].

Sample	**Zr wt%**	**Zn wt%**	**Zr : Zn**
(UiO-66)(a_gZIF-UC-7)(50/50)	4.710	5.730	1 : 1.22
[(UiO-66)$_{0.5}$(a_gZIF-UC-7)$_{0.5}$]	9.296	12.226	1 : 1.32

Table S7. Calculated composition by weight of (UiO-66)(a_gZIF-UC-7)(50/50)and [(UiO-66)$_{0.5}$(a_gZIF-UC-7)$_{0.5}$].

	(UiO-66)(a_gZIF-UC-7)(50/50)		**[(UiO-66)$_{0.5}$(a_gZIF-UC-7)$_{0.5}$]**	
Method	**X**	**y**	**x**	**1-x**
CHN			0.50	0.50
ICP	58	42	0.60	0.40

4.3 Scanning electron microscopy

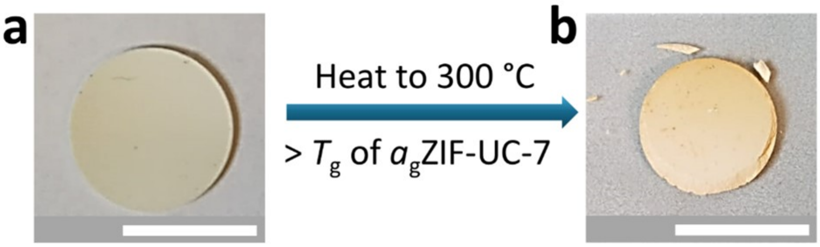

Figure S17. Photographs of **a.** Pelletised (UiO-66)(a_gZIF-UC-7)(50/50) physical mixture (*i.e.*, ball-milled and pelletised starting materials prior to heating), **b.** [(UiO-66)$_{0.5}$(a_gZIF-UC-7)$_{0.5}$] composite. Scale bar is 1 mm.

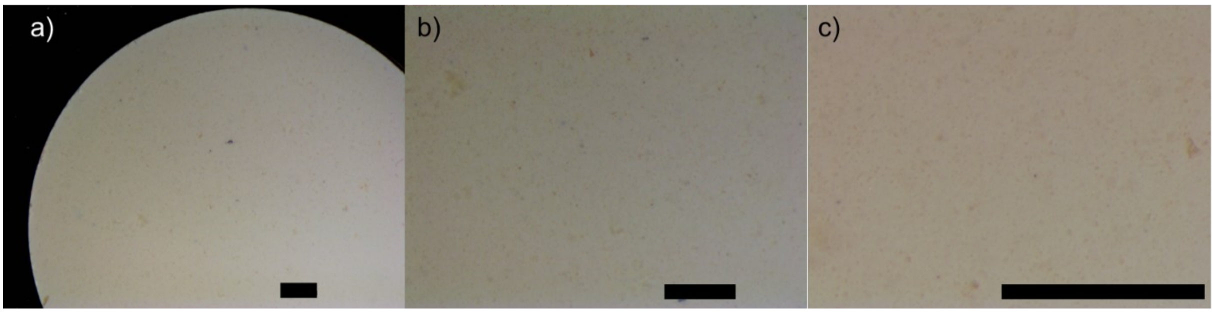

Figure S18. Optical images of the pelletised (UiO-66)(a_gZIF-UC-7)(50/50) physical mixture. Scale bars: 1 mm.

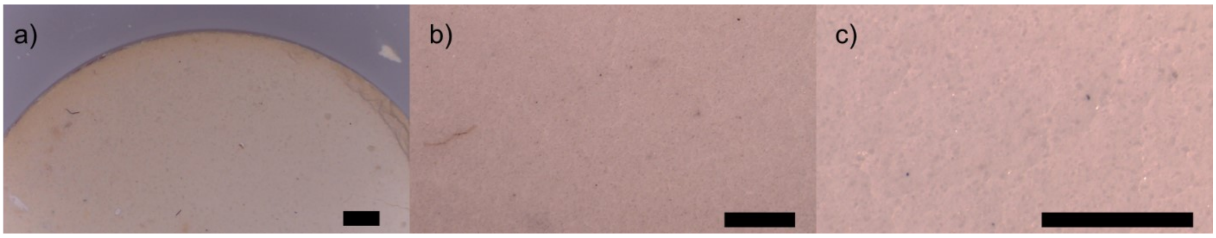

Figure S19. Optical images of the composite (material after the thermal treatment). Scale bars: 1 mm.

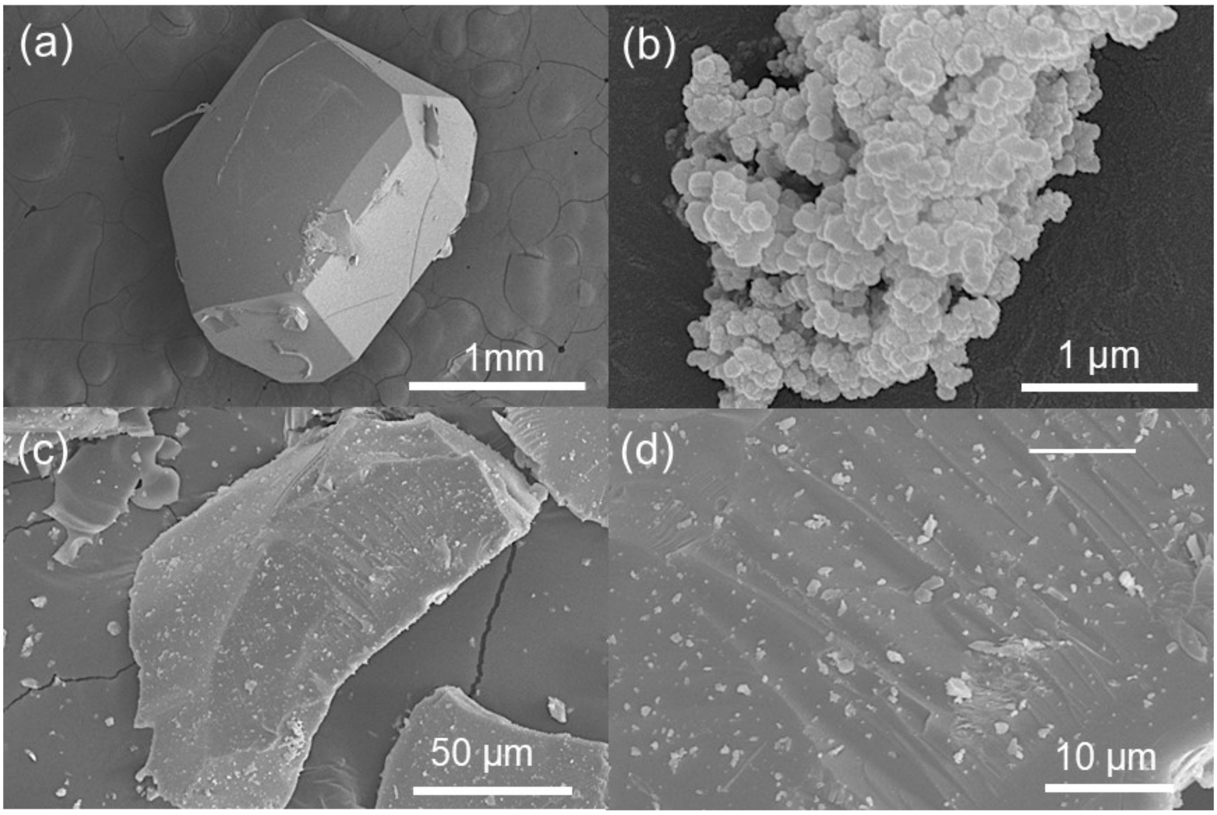

Figure S20. SEM images of **a.** ZIF-UC-7 single crystal (35 x), **b.** UiO-66 (35 000 x), **c.** a_gZIF-UC-7 (650 x) and **d.** a_gZIF-UC-7 (2500 x). Magnification is given in brackets.

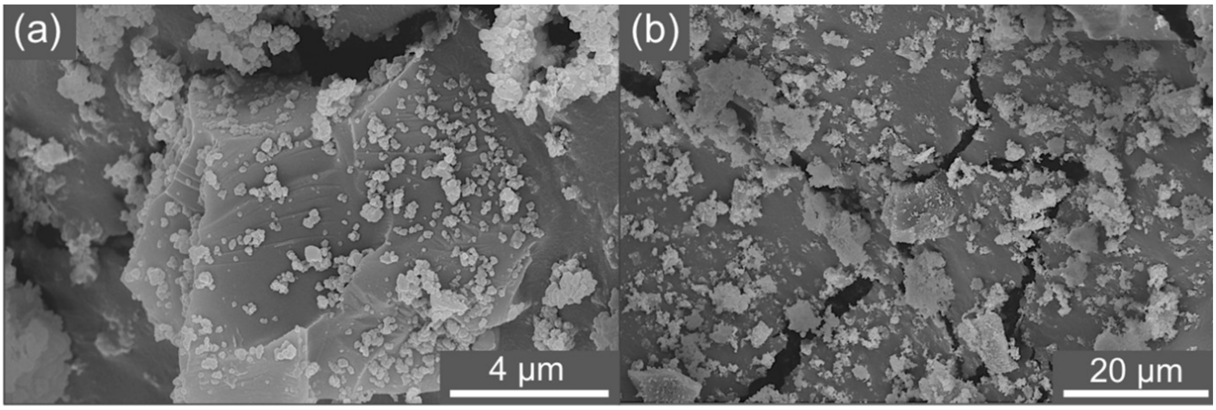

Figure S21. SEM images of the (UiO-66)(a_gZIF-UC-7)(50/50) physical mixture at **a.** 8000 x and **b.** 1500 x magnification.

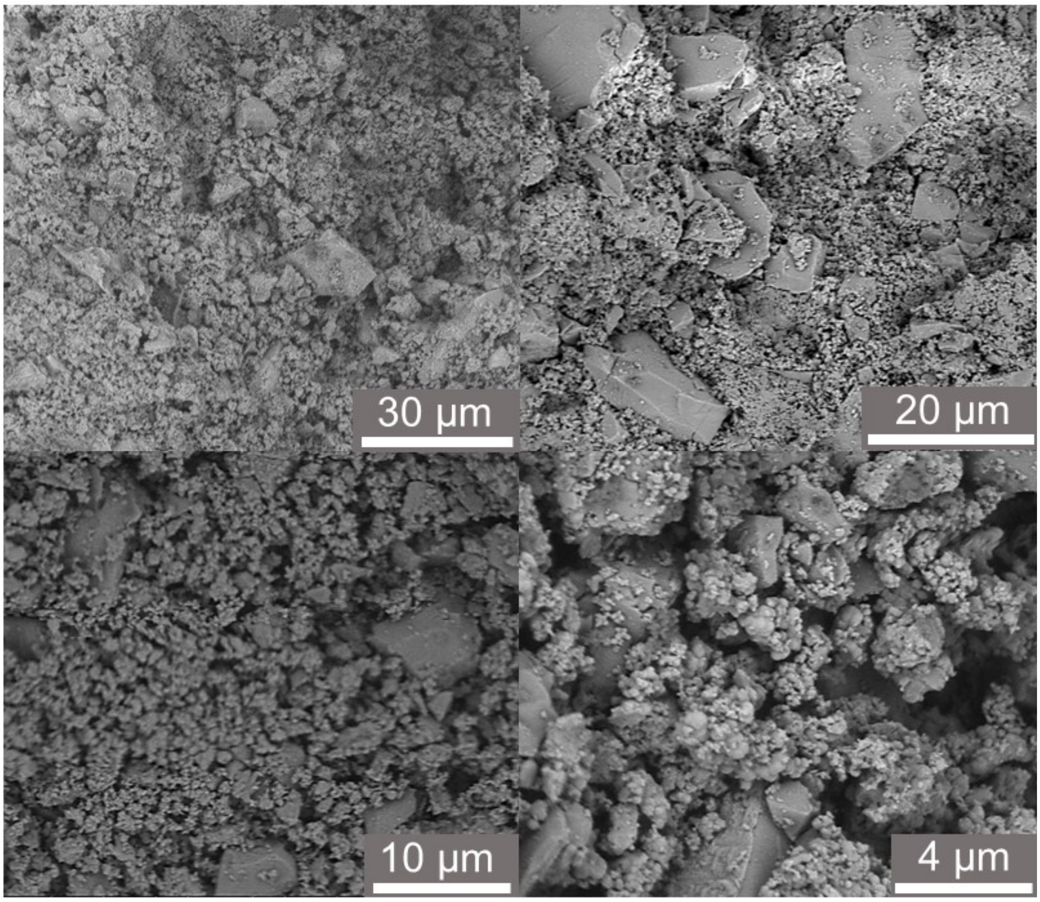

Figure S22. SEM images of the pelletised (UiO-66)(a_gZIF-UC-7)(50/50) physical mixture.

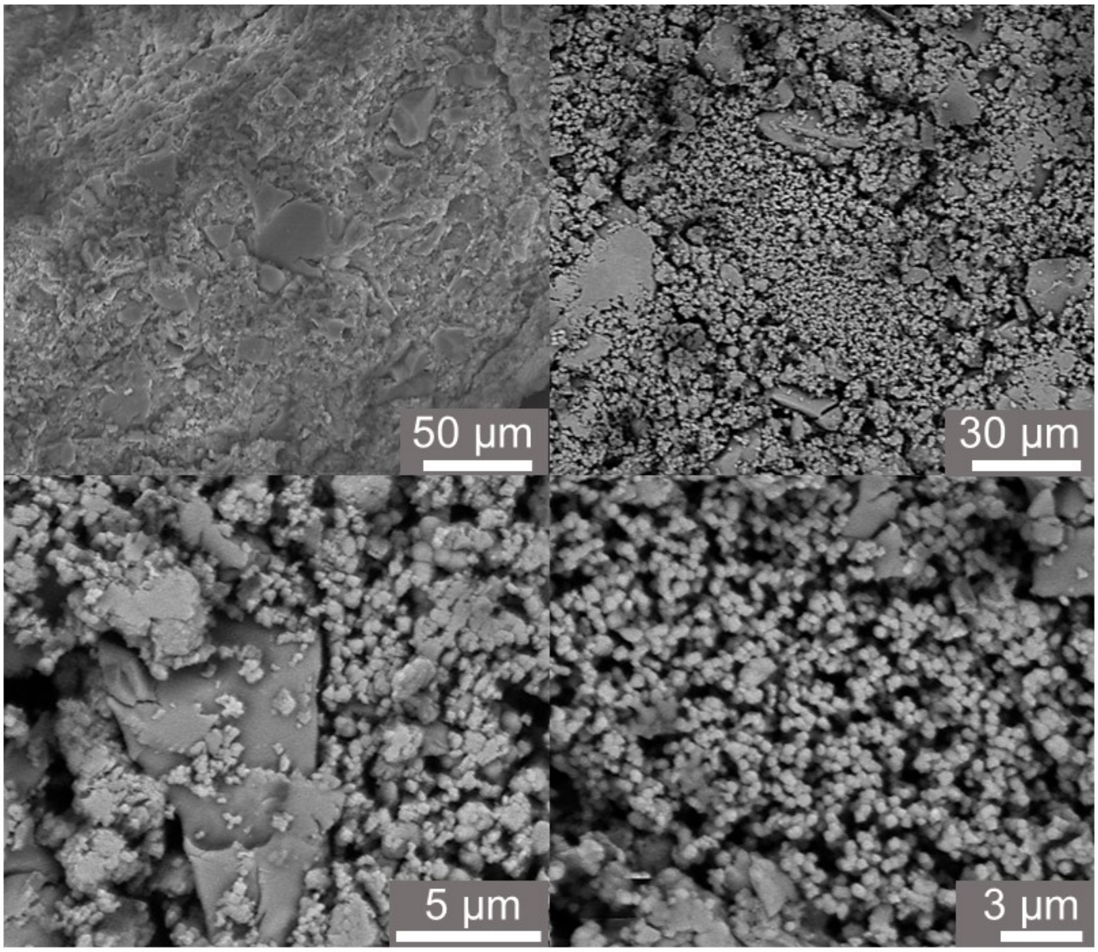

Figure S23. SEM images of the [(UiO-66)$_{0.5}$(a_gZIF-UC-7)$_{0.5}$] composite.

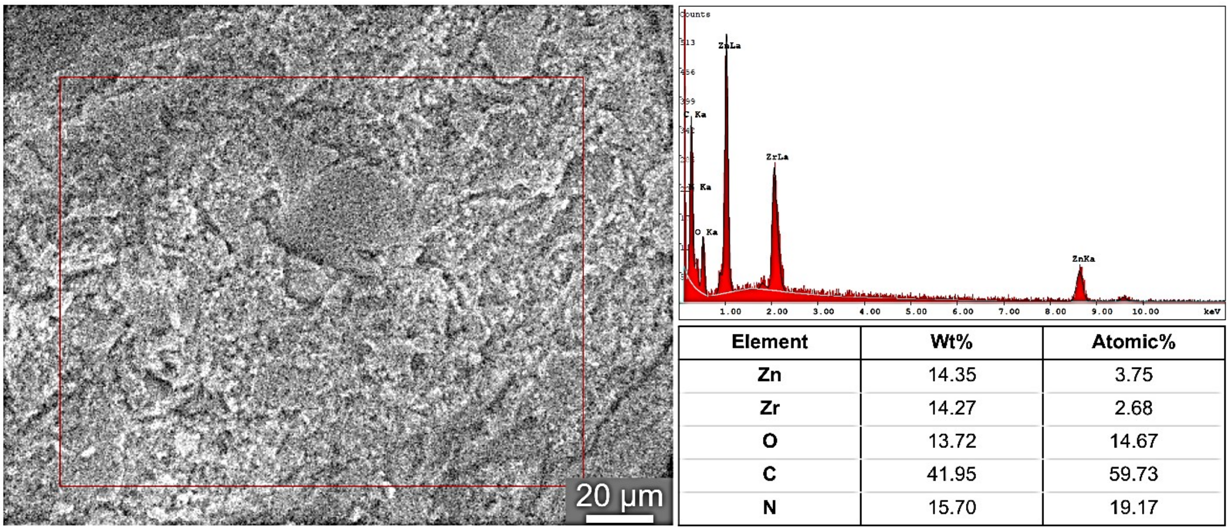

Element	Wt%	Atomic%
Zn	14.35	3.75
Zr	14.27	2.68
O	13.72	14.67
C	41.95	59.73
N	15.70	19.17

Figure S24. EDX compositional analysis of a region of the pelletised (UiO-66)(a_gZIF-UC-7)(50/50) physical mixture.

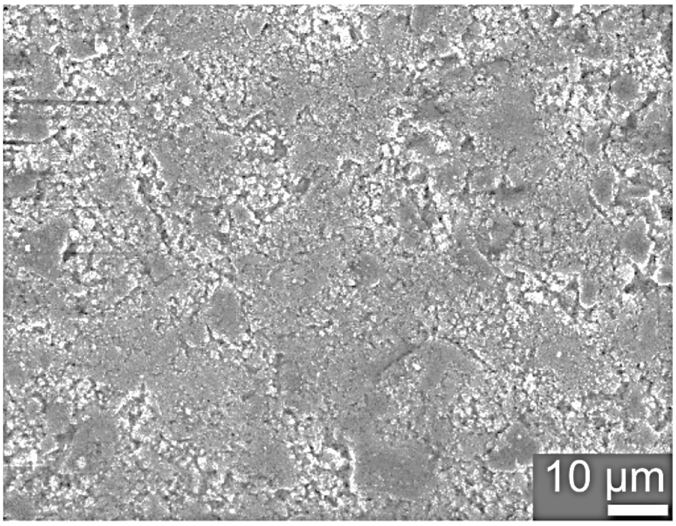

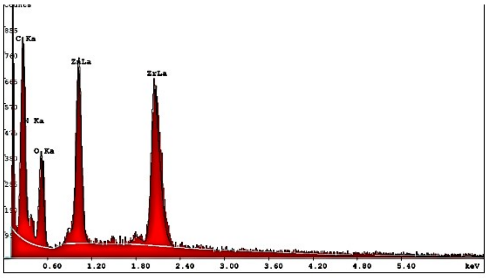

Element	Wt%	Atomic%
Zn	16.72	4.52
Zr	14.51	2.81
O	16.37	18.06
C	40.98	60.23
N	11.41	14.38

Figure S25. EDX compositional analysis of a region of the [(UiO-66)$_{0.5}$(a_gZIF-UC-7)$_{0.5}$] composite.

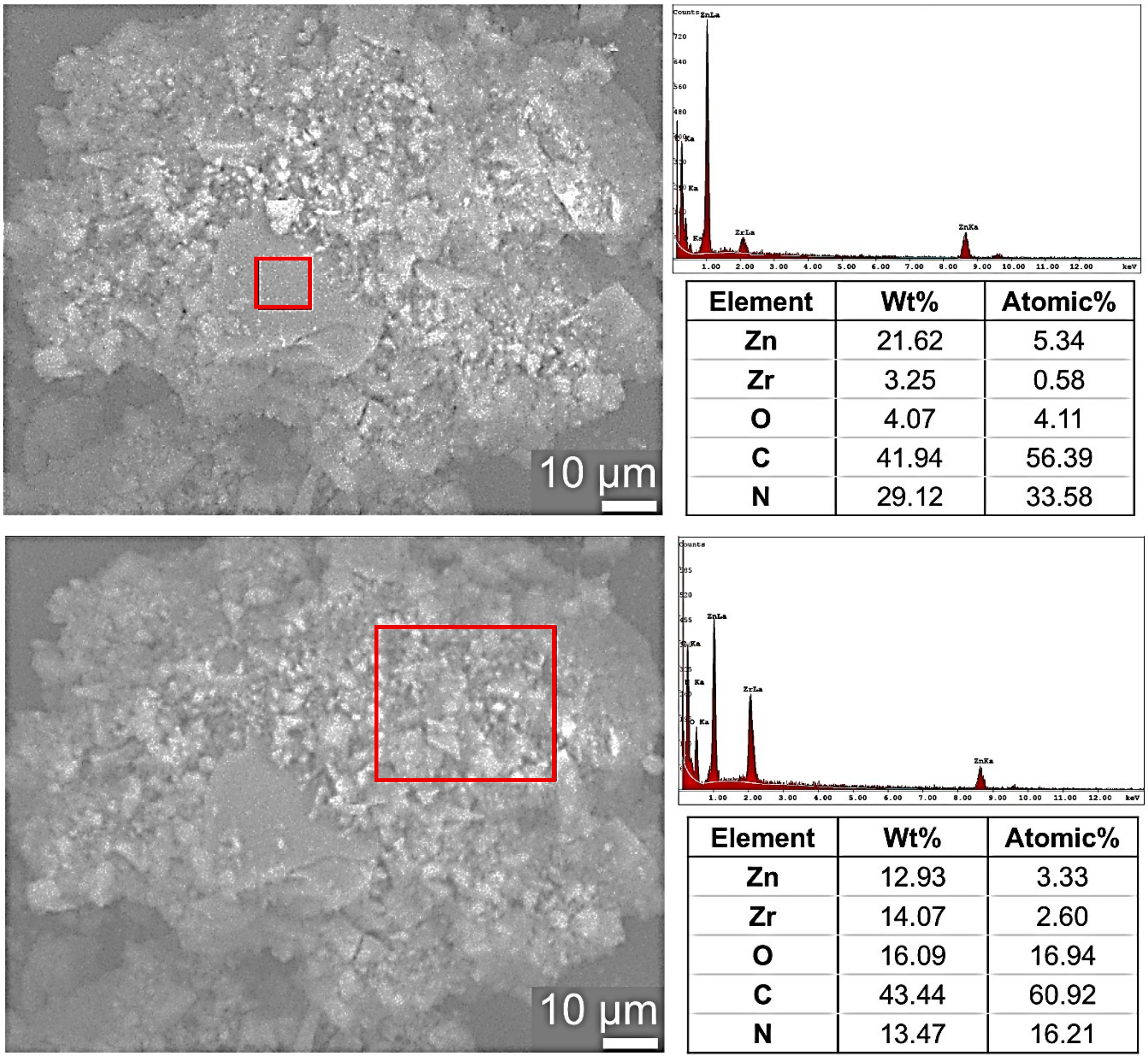

Element	Wt%	Atomic%
Zn	21.62	5.34
Zr	3.25	0.58
O	4.07	4.11
C	41.94	56.39
N	29.12	33.58

Element	Wt%	Atomic%
Zn	12.93	3.33
Zr	14.07	2.60
O	16.09	16.94
C	43.44	60.92
N	13.47	16.21

Figure S26. EDX compositional analysis of a different region of the [(UiO-66)$_{0.5}$(a_gZIF-UC-7)$_{0.5}$] composite. Red rectangle on the top image focuses on a region of a_gZIF-UC-7 glass, demonstrated by lower atomic ratios of O and Zr and a Zr: Zn ratio of 1: 9.2. The red rectangle on the bottom image corresponds to UiO-66 crystallites, given by higher atomic ratios of O and Zr and a Zr: Zn ratio of 1: 1.3.

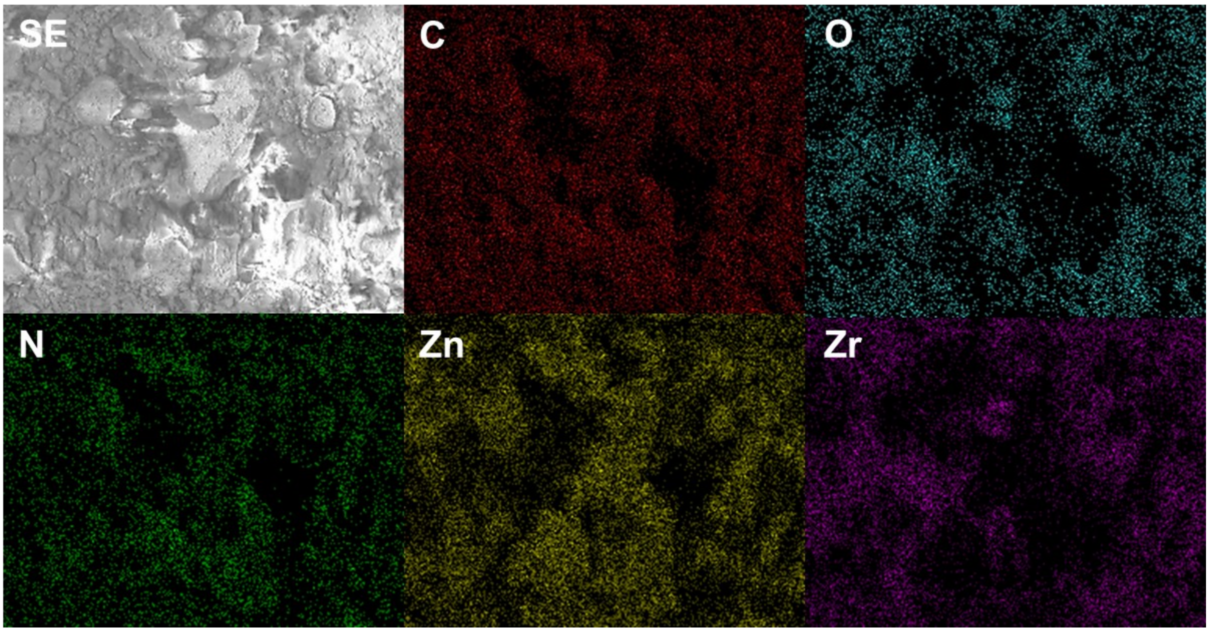

Figure S27. EDX mapping of the composite showing the bulk of the pellet of the [(UiO-66)$_{0.5}$(a_gZIF-UC-7)$_{0.5}$] composite. Magnification: 5054. Energy: 20 KeV.

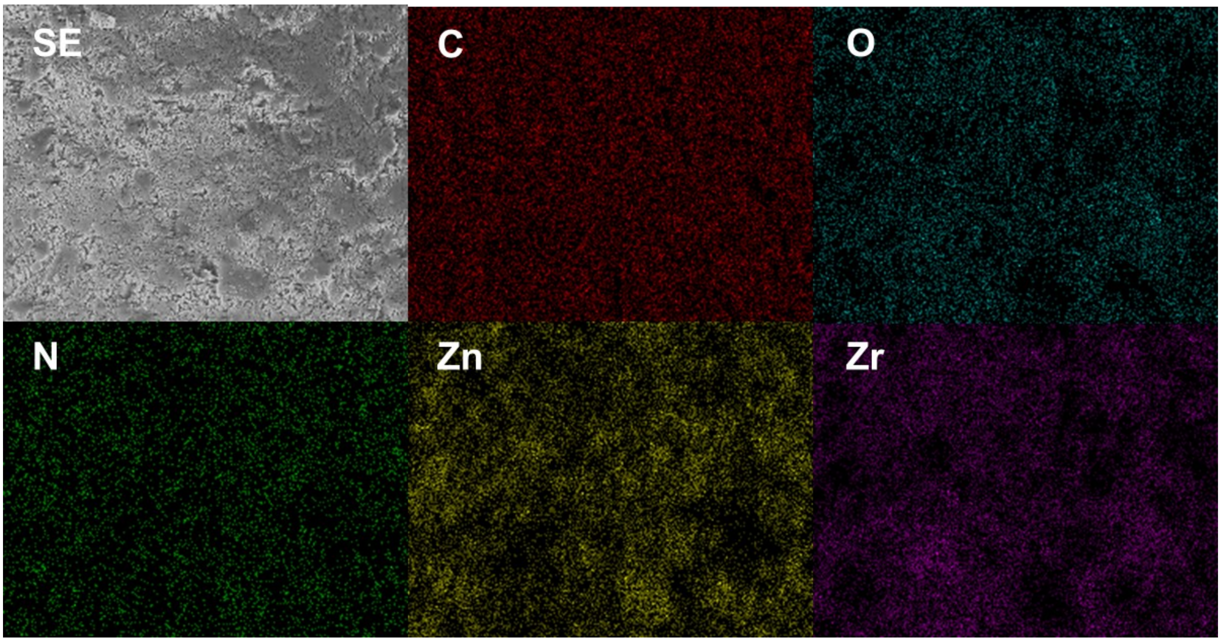

Figure S28. EDX mapping of the composite showing the surface of the pellet of the [(UiO-66)$_{0.5}$(a_gZIF-UC-7)$_{0.5}$] composite. Magnification: 2800. Energy: 20 KeV.

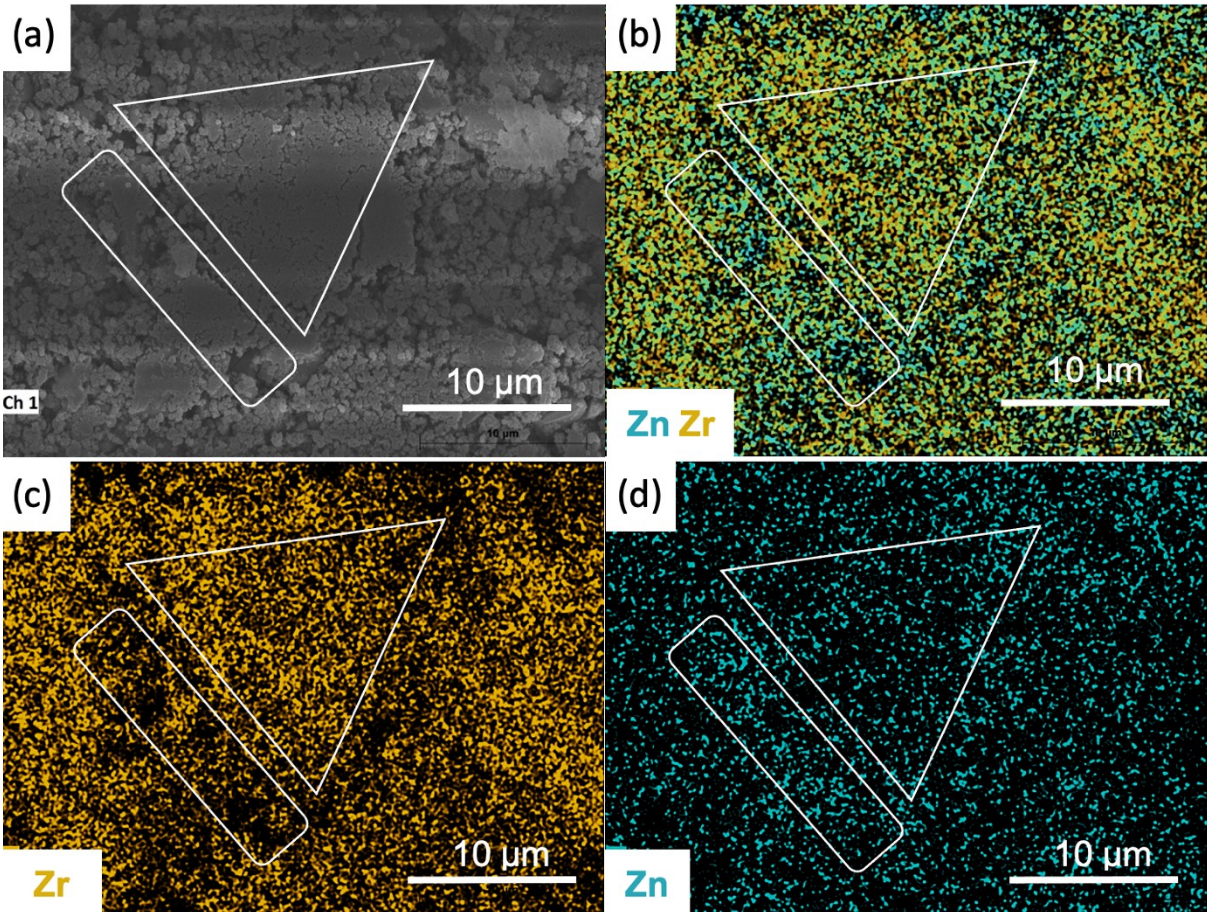

Figure S29. a. SEM image and **b-d.** EDX mapping of the [(UiO-66)$_{0.5}$(a_gZIF-UC-7)$_{0.5}$] composite showing the surface of the pellet.

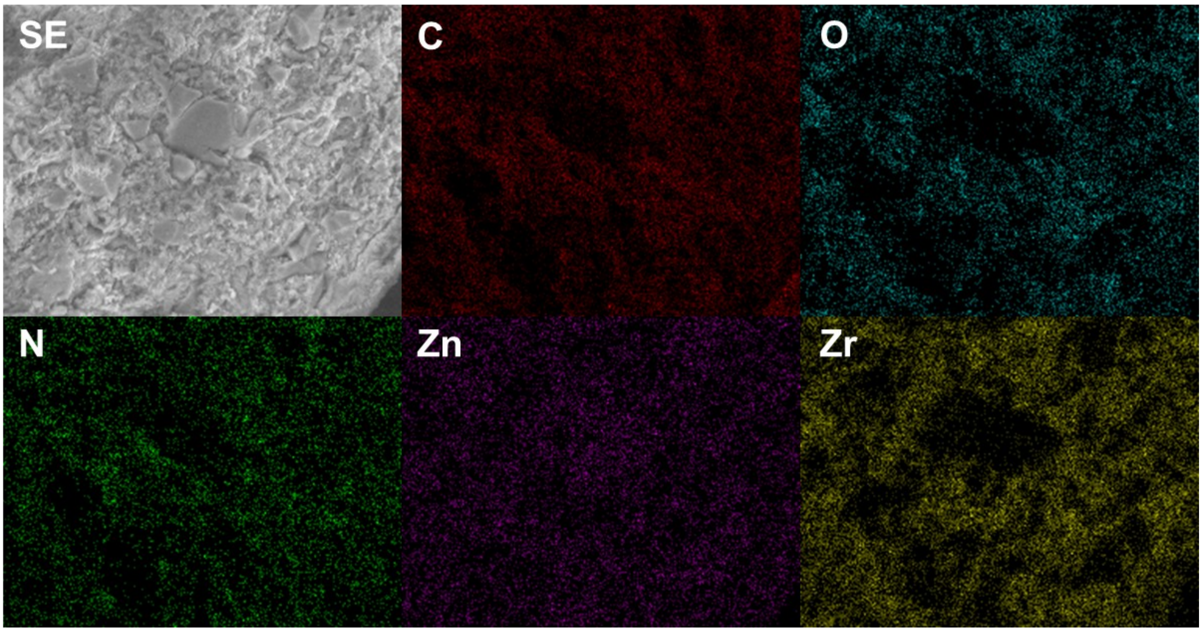

Figure S30. EDX mapping of the composite showing the surface of the pelletised (UiO-66)(a_gZIF-UC-7)(50/50) physical mixture. Magnification: 1566. Energy: 20KeV.

4.4 Pair distribution function

The $S(Q)$s of the starting materials show Bragg scattering for UiO-66 and a lack of long-range order for a_gZIF-UC-7.

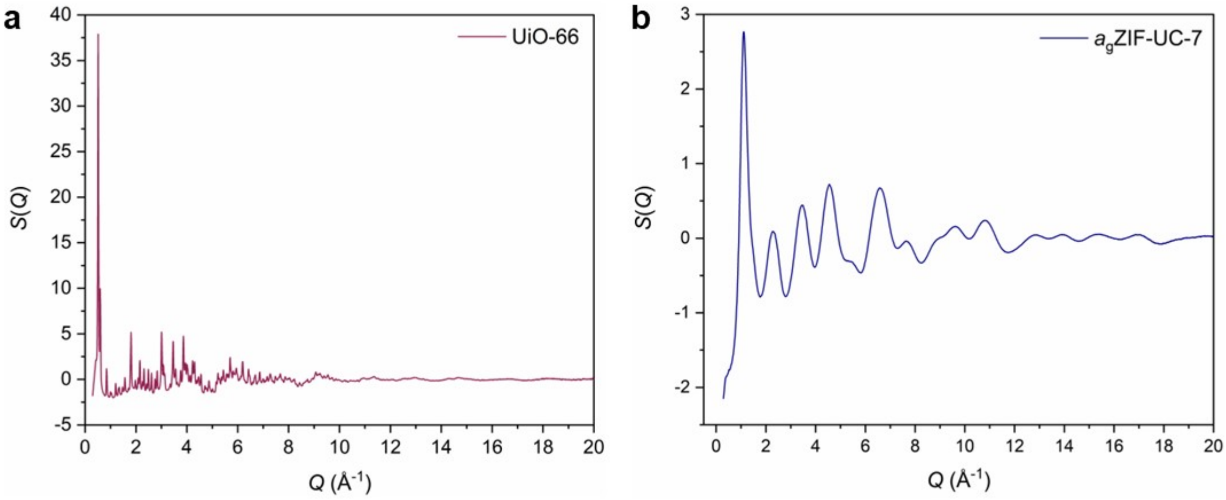

Figure S31. $S(Q)$s of **a.** UiO-66 and **b.** a_gZIF-UC-7.

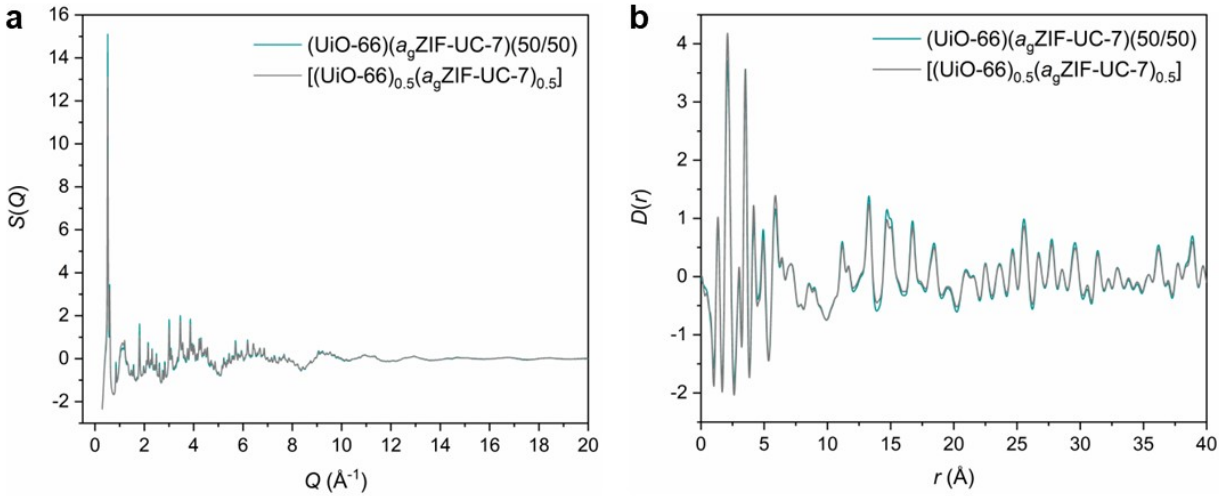

Figure S32. a. $S(Q)$s and **b.** $D(r)$s of the (UiO-66)(a_gZIF-UC-7)(50/50) physical mixture and [(UiO-66)$_{0.5}$(a_gZIF-UC-7)$_{0.5}$] composite.

The $D(r)$ of UiO-66 is consistent with its crystal structure, showing main Zr–Zr and Zr–O $Zr_6O_4(OH)_4$ cluster correlations 1-6 (**Figure S33.a**) below 8 Å.[7,8] Between ~6.4 Å and ~9 Å, there are overlapping peak contributions from Zr–C atom pairs which leads to peak broadening and an overall absence of distinct peaks in this region. Correlations 7-11 Å correspond to intercluster bond distances (**Figure S33.b**).

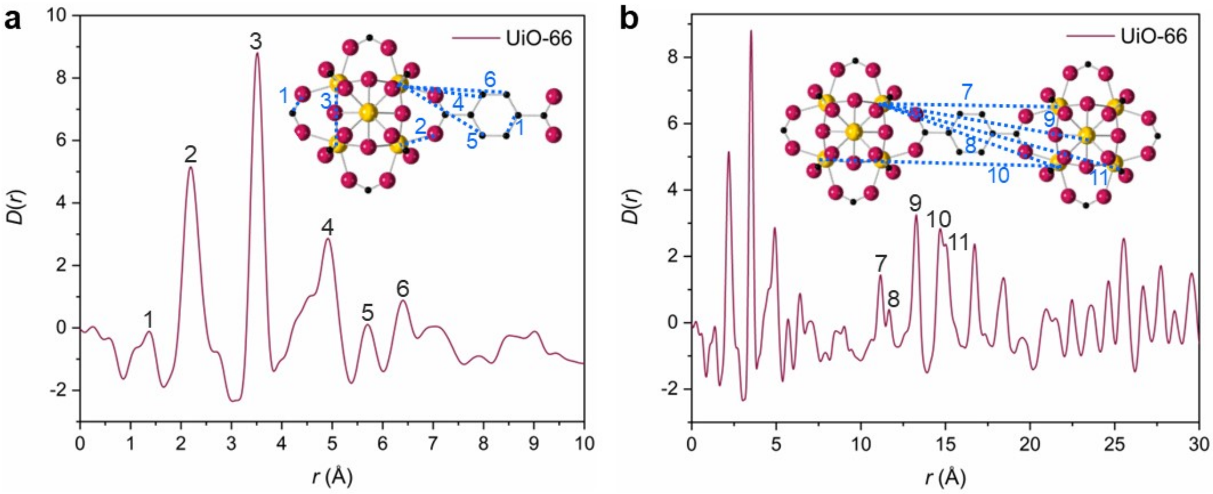

Figure S33. X-ray PDF of UiO-66 in a *r* range of **a.** 0-10 Å, inset shows a $Zr_6O_4(OH)_4$ cluster and BDC linker and **b.** 0-30 Å, inset shows two $Zr_6O_4(OH)_4$ clusters linked by a BDC linker. Correlations 1 (C-C, C-O), 2 (Zr-O), 3 (Zr-Zr intracluster distance), 4-6 (Zr-C), 7-11 (Zr-Zr intercluster bond distances). Zr-yellow, C-black, O-pink; hydrogen atoms omitted for clarity.

The *D*(*r*) of a_gZIF-UC-7 shows key correlations A-E originating from the imidazolate linker (**Figure S34**), consistent with the crystal structure of ZIF-UC-7 and other imidazolate-containing ZIFs.[5] Only small features are visible above ~ 6 Å because of the glass' lack of long-range order.

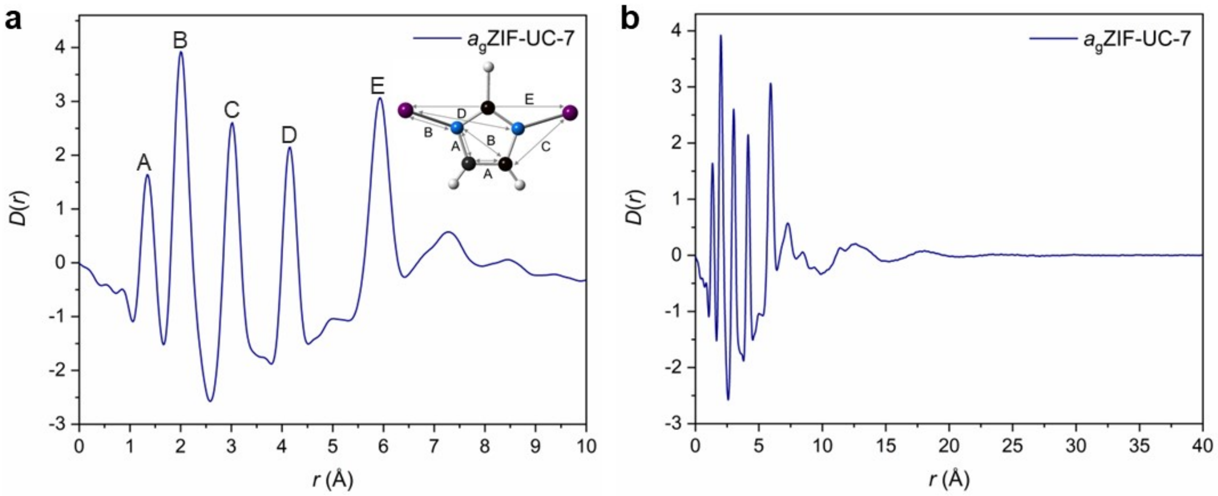

Figure S34. X-ray PDF of a_gZIF-UC-7 at **a.** *r* = 0-10 Å and **b.** *r* = 0-40 Å. Inset shows the main correlations A-E of the imidazolate linker.

4.5 Thermal analysis

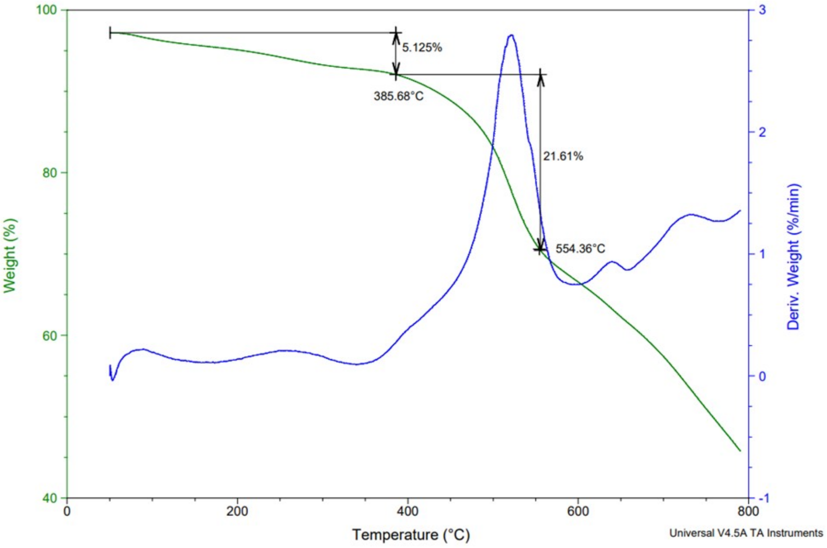

Figure S35. TGA of the (UiO-66)(a_gZIF-UC-7)(50/50) physical mixture.

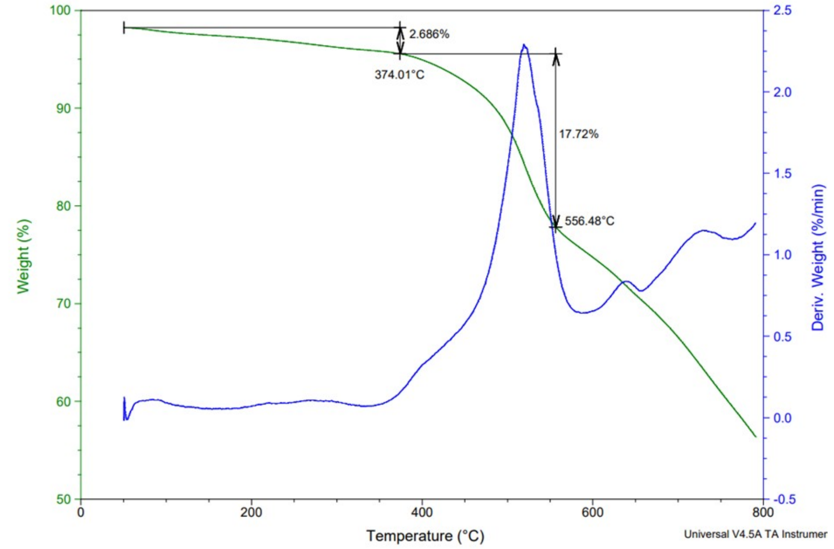

Figure S36. TGA of the [(UiO-66)$_{0.5}$(a_gZIF-UC-7)$_{0.5}$] composite.

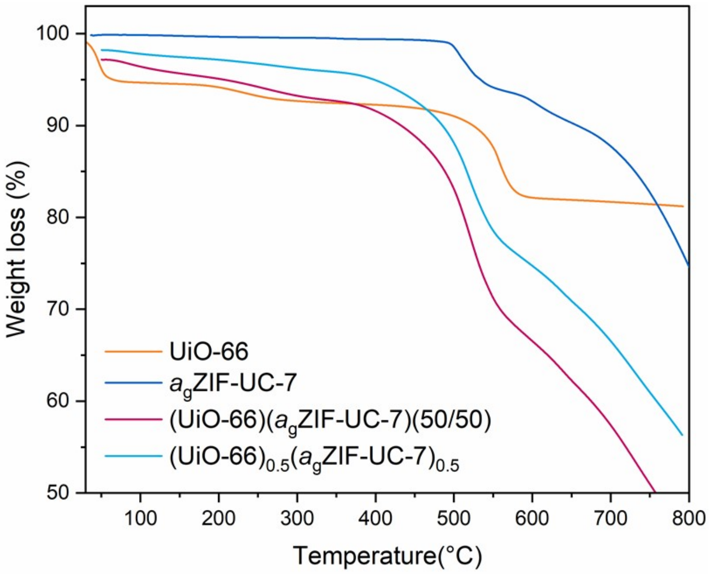

Figure S37. TGA curves of the (UiO-66)(a_gZIF-UC-7)(50/50) physical mixture, $[(UiO-66)_{0.5}(a_gZIF-UC-7)_{0.5}]$ composite and starting materials.

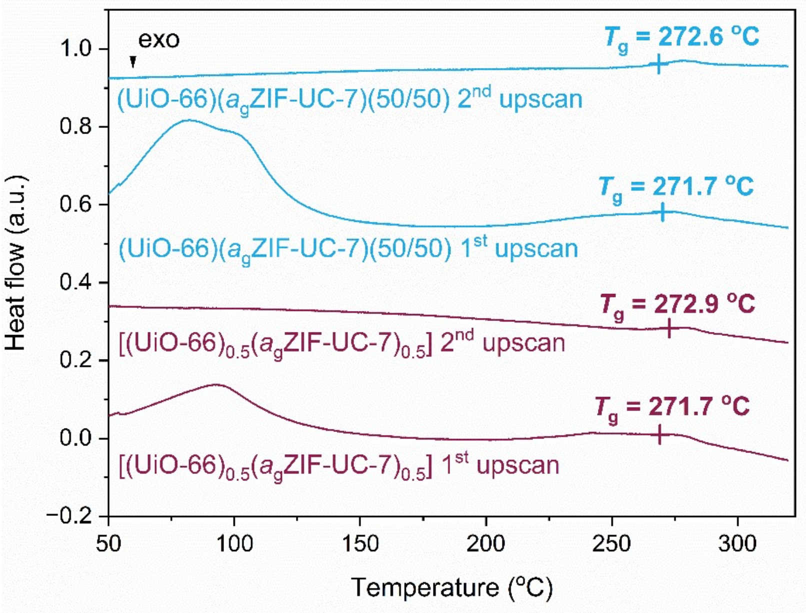

Figure S38. 1st and 2nd DSC upscan of physical mixture (pink) stacked with that of the composite (blue). An endothermic feature is present between 50 and ~130 °C in the first upscans of both the physical mixture and composite corresponding to surface water loss from the UiO-66. This endothermic peak was smaller in the $[(UiO-66)_{0.5}(a_gZIF-UC-7)_{0.5}]$ compared to the physical mixture, suggesting water removal during composite fabrication. Water loss was evident in the TGA of UiO-66 (Fig S11).

4.6 Composite properties

Table S8. Gas sorption summary for all the materials.

Material	CO_2 STP (cm^3 g^{-1})	N_2 STP (cm^3 g^{-1})	BET (m^2 g^{-1})
ZIF-UC-7	51.1	41.81	50.92 ± 0.22
a_gZIF-UC-7	14.77	55.37	98.74 ± 0.95
UiO-66	95.03	378.46	852.68 ± 8
[(UiO-66)$_{0.5}$(a_gZIF-UC-7)$_{0.5}$]	30.94	111.38	214.01 ± 1.33
Pelletised (UiO-66)(a_gZIF-UC-7)(50/50) physical mixture	NA	110.78	220.63 ± 1.23
[(UiO-66)$_{0.5}$(a_gZIF-UC-7)$_{0.5}$]-PBS	NA	98.54	182.30 ± 0.18

Table S9. N_2 gas sorption summary for the tested materials and literature glass-forming ZIFs.

Material	N_2 STP (mmol g^{-1})		Reference
	Crystalline	Glass	
ZIF-UC-7	1.85	2.48	This work
UiO-66	13.1	NA	[9]
[(UiO-66)$_{0.5}$(a_gZIF-UC-7)$_{0.5}$]	4.74	NA	This work
ZIF-62	0.49	0.57	[9]
ZIF-4	8.57	0.91	[9]
TIF-4	0.54	0.18	[9]
zni-ZIF-4	0.73	0.72	[9]

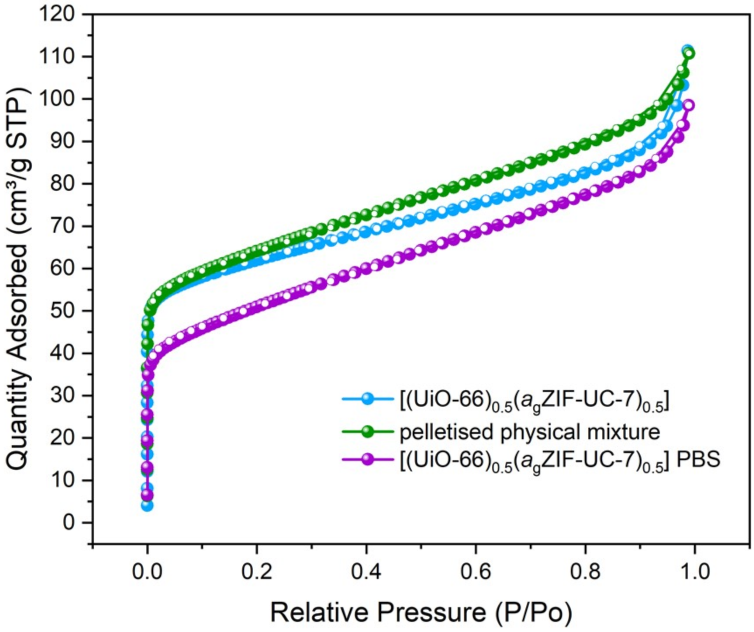

Figure S39. Comparison of the N_2 gas sorption isotherms of the pelletised (UiO-66)(a_gZIF-UC-7)(50/50) physical mixture, composite and the composite after the PBS immersion.

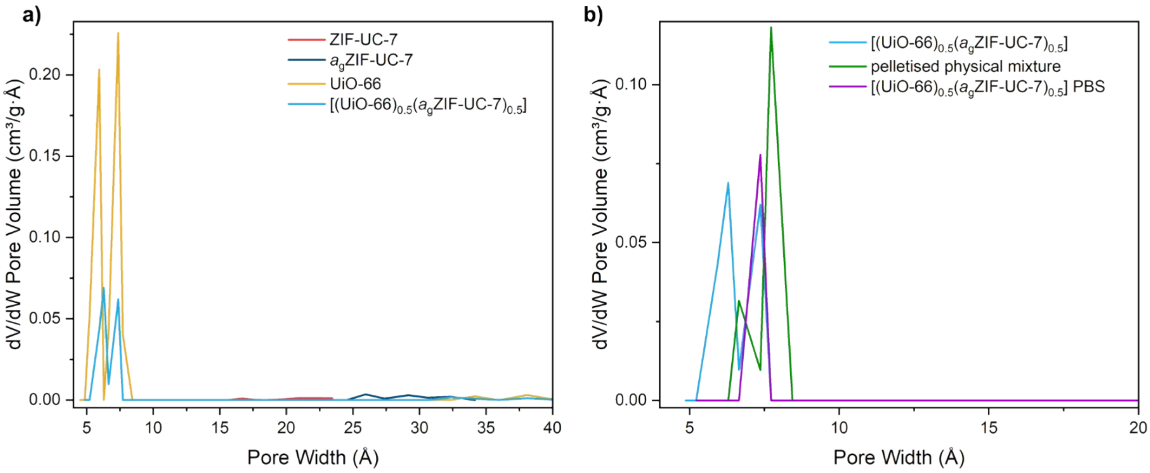

Figure S40. a. Comparison of the stacked pore size distributions of all the materials. **b.** Comparison of the pore size distribution of the pelletised (UiO-66)(a_gZIF-UC-7)(50/50) physical mixture, after the thermal treatment (composite) and after its immersion in PBS for 24-hours.

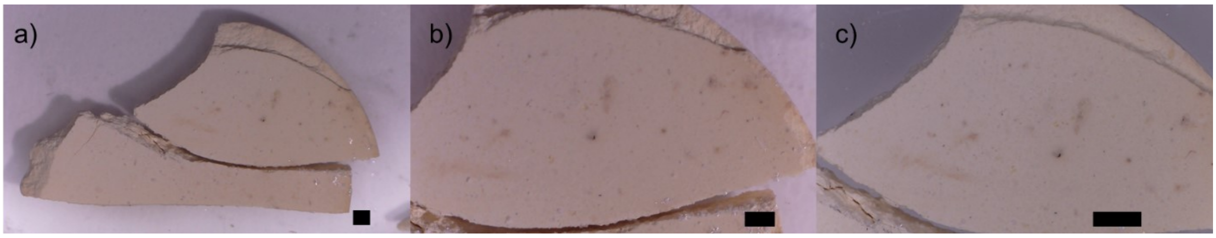

Figure S41. Optical images of the composite after its immersion in PBS for 24-hours. Scale bars: 1 mm.

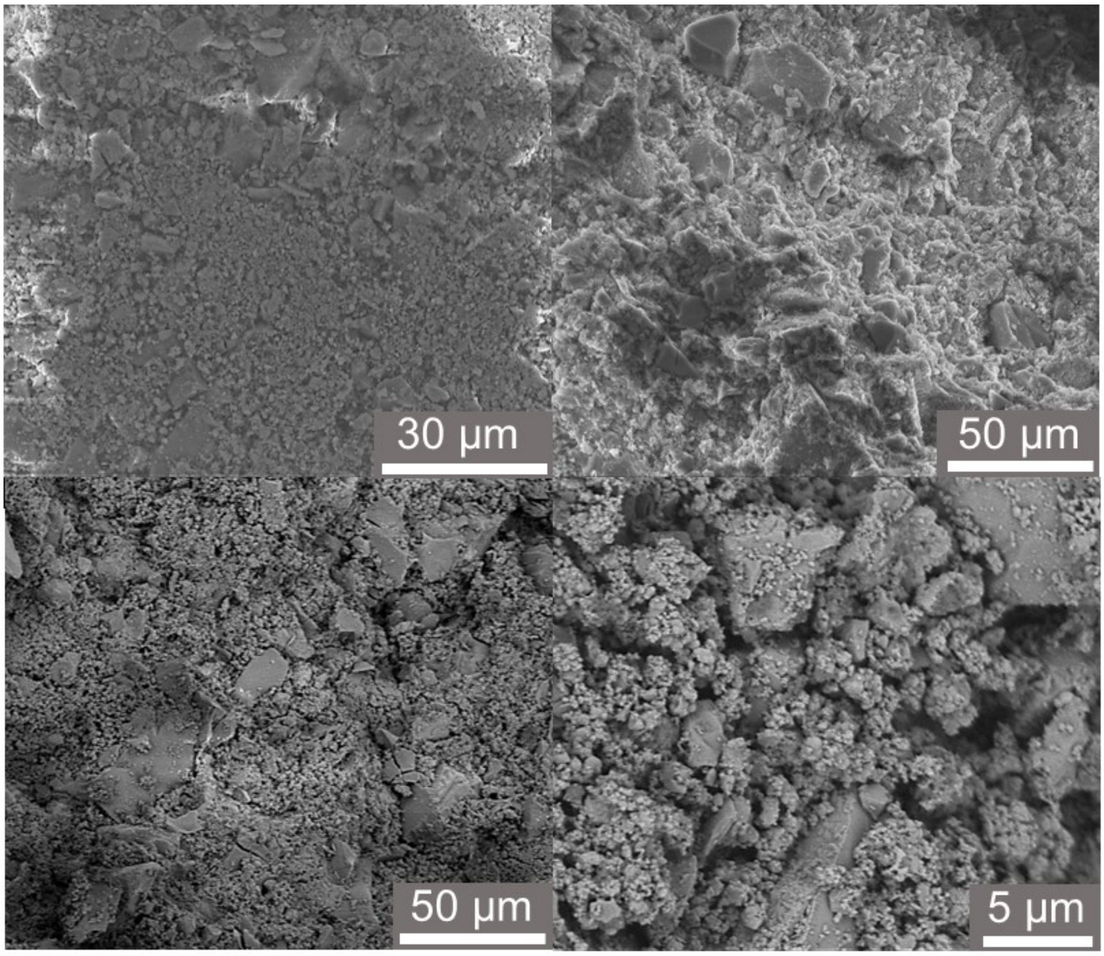

Figure S42. SEM images of the [(UiO-66)$_{0.5}$(a_gZIF-UC-7)$_{0.5}$] composite after 24-hour immersion in PBS solution.

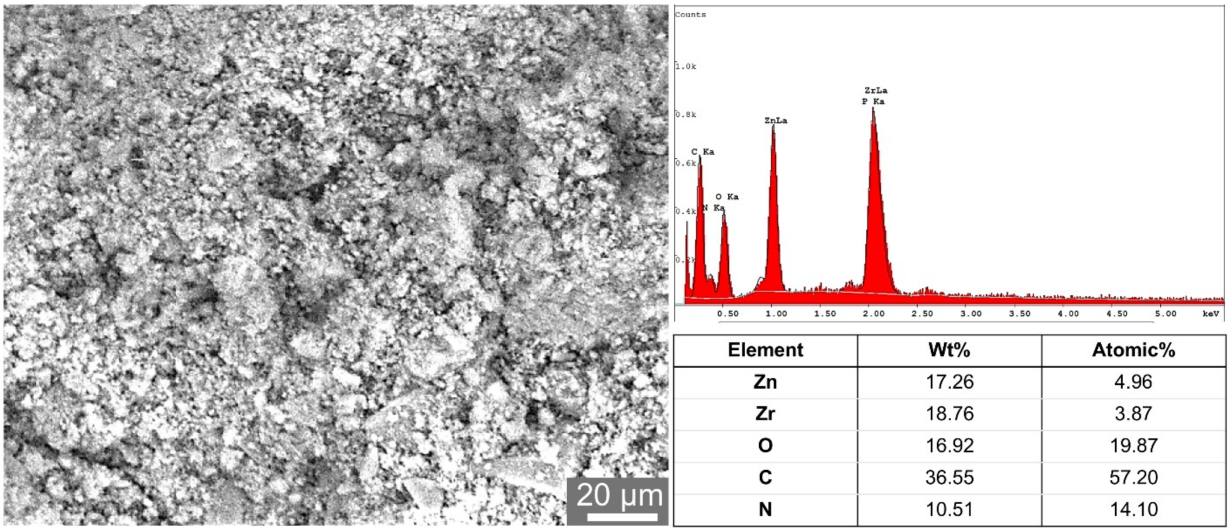

Element	Wt%	Atomic%
Zn	17.26	4.96
Zr	18.76	3.87
O	16.92	19.87
C	36.55	57.20
N	10.51	14.10

Figure S43. EDX compositional analysis of a region of the [(UiO-66)$_{0.5}$(a_gZIF-UC-7)$_{0.5}$] composite after 24-hour immersion in PBS solution.

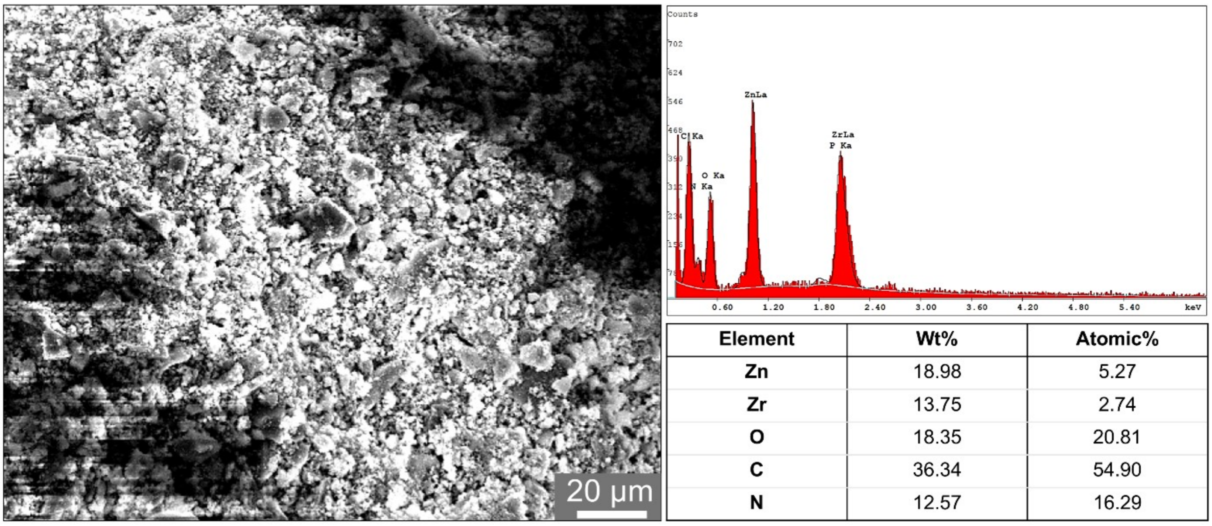

Element	Wt%	Atomic%
Zn	18.98	5.27
Zr	13.75	2.74
O	18.35	20.81
C	36.34	54.90
N	12.57	16.29

Figure S44. EDX compositional analysis of a different region of the [(UiO-66)$_{0.5}$(a_gZIF-UC-7)$_{0.5}$] composite after 24-hour immersion in PBS solution.

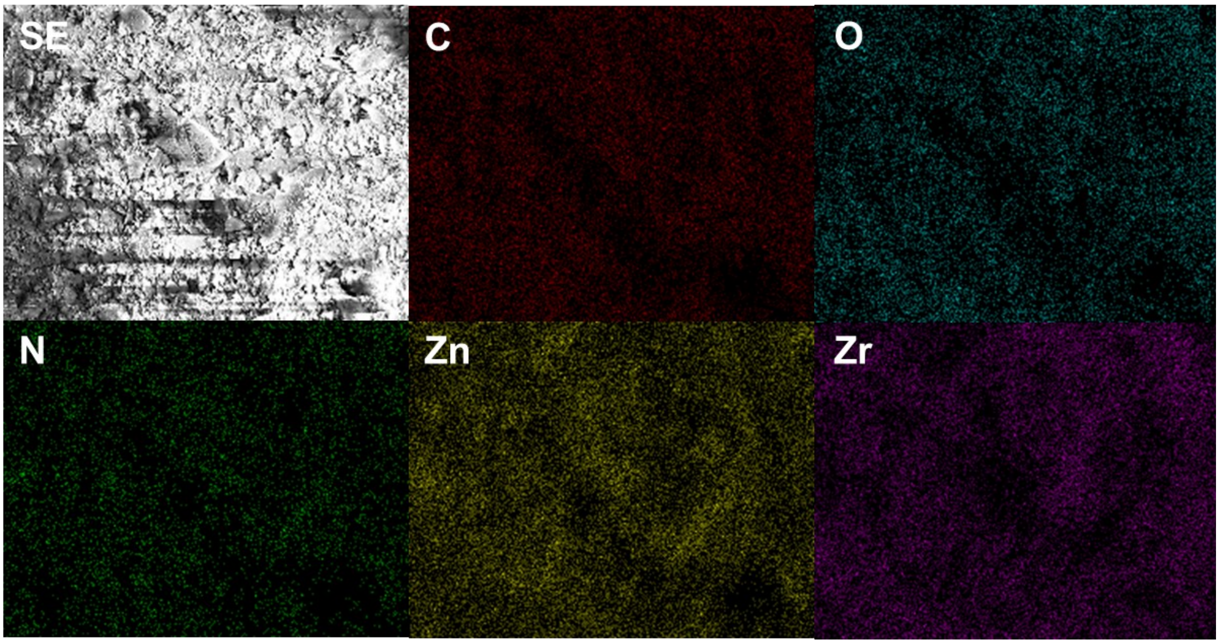

Figure S45. EDX mapping of the composite showing the surface of [(UiO-66)$_{0.5}$(a_gZIF-UC-7)$_{0.5}$] composite after 24-hour immersion in PBS solution. Magnification: 3000. Energy: 20KeV.

Table S10. ICP-OES microanalysis of the [(UiO-66)$_{0.5}$(a_gZIF-UC-7)$_{0.5}$] composite and the of the [(UiO-66)$_{0.5}$(a_gZIF-UC-7)$_{0.5}$] composite after immersion in PBS for 24 hours. Total weight of the [(UiO-66)$_{0.5}$(a_gZIF-UC-7)$_{0.5}$] composite before the immersion: 101.2 mg, total weight of the [(UiO-66)$_{0.5}$(a_gZIF-UC-7)$_{0.5}$] composite after immersion in PBS for 24 hours: 99.3 mg.

Sample	**Zr (ppm)**	**Zn (ppm)**	**P (ppm)**	**Zr : Zn**
[(UiO-66)$_{0.5}$(a_gZIF-UC-7)$_{0.5}$]	6.863 ± 0.094	8.462 ± 0.157	0.02 ± 0.01	1 : 1.23
[(UiO-66)$_{0.5}$(a_gZIF-UC-7)$_{0.5}$] post immersion	4.407 ± 0.079	4.734 ± 0.067	0.143 ± 0.005	1 : 1.07
PBS Supernatant	0.298 ± 0.003	0.518 ± 0.007	115.2 ± 0.97	1: 1.74
PBS	N.A	N.A	137.1 ± 3.34	N.A

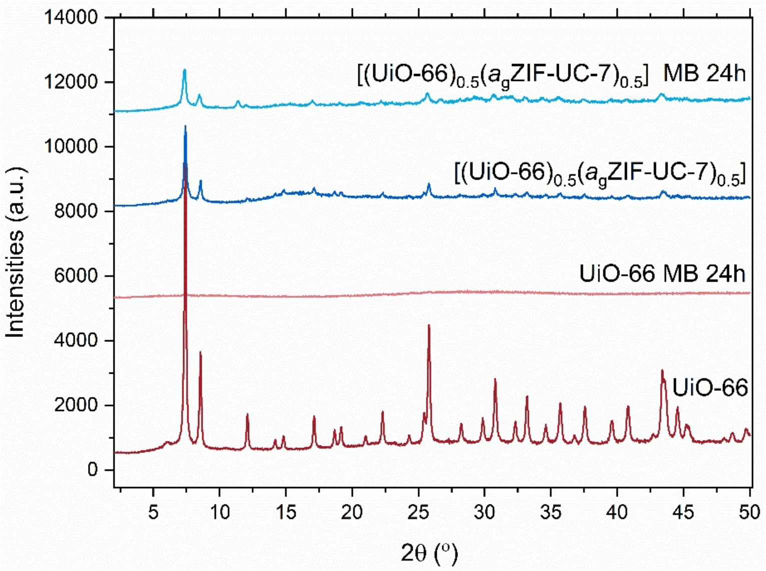

Figure S46. PXRD patterns of UiO-66 and the [(UiO-66)$_{0.5}$(a_gZIF-UC-7)$_{0.5}$] composite after 24-hour immersion in PBS solutions containing 5 ppm of methylene blue.

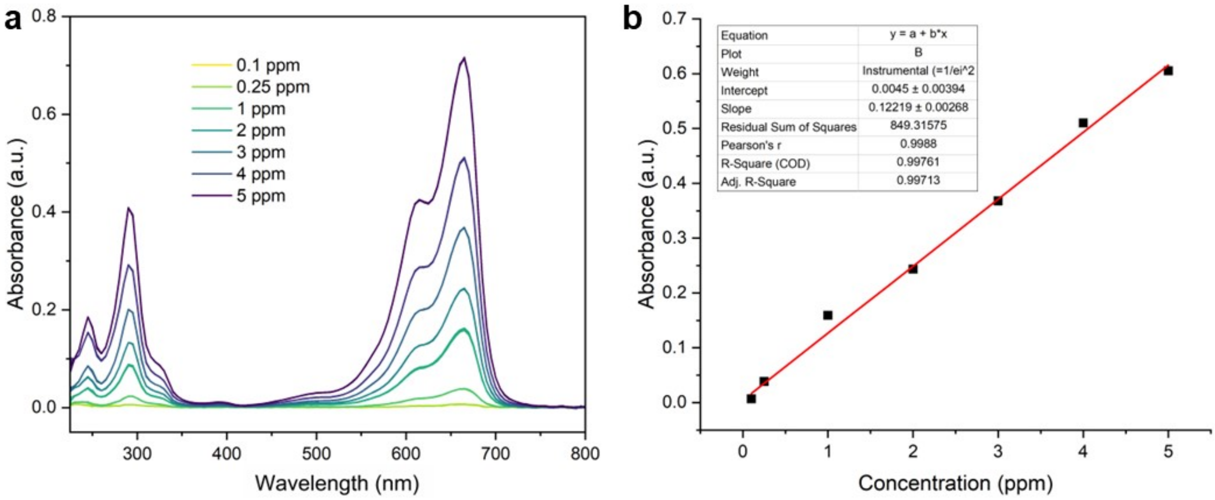

Equation	y = a + b*x
Plot	B
Weight	Instrumental (=1/ei^2
Intercept	0.0045 ± 0.00394
Slope	0.12219 ± 0.00268
Residual Sum of Squares	849.31575
Pearson's r	0.9988
R-Square (COD)	0.99761
Adj. R-Square	0.99713

Figure S47. **a.** UV-VIS spectra of variable MB concentrations in PBS used for the calibration curve and **b.** The determined calibration curve of UV-VIS absorption data for MB in PBS.

5. References

1 A. A. Coelho, *J. Appl. Crystallogr.*, 2018, **51**, 210–218.

2 A. K. Soper, *GudrunN and GudrunX: programs for correcting raw neutron and X-ray diffraction data to differential scattering cross section*, 2011.

3 A. K. Soper and E. R. Barney, *J. Appl. Crystallogr.*, 2011, **44**, 714–726.

4 D. A. Keen, *J. Appl. Crystallogr.*, 2001, **34**, 172–177.

5 A. M. Bumstead, C. Castillo-Blas, I. Pakamorė, M. F. Thorne, A. F. Sapnik, A. M. Chester, G. Robertson, D. J. M. Irving, P. A. Chater, D. A. Keen, R. S. Forgan and T. D. Bennett, *Chem. Commun.*, 2023, **59**, 732–735.

6 Y. Ma, X. Han, S. Xu, Z. Wang, W. Li, I. da Silva, S. Chansai, D. Lee, Y. Zou, M. Nikiel, P. Manuel, A. M. Sheveleva, F. Tuna, E. J. L. McInnes, Y. Cheng, S. Rudić, A. J. Ramirez-Cuesta, S. J. Haigh, C. Hardacre, M. Schröder and S. Yang, *J. Am. Chem. Soc.*, 2021, **143**, 10977–10985.

7 T. D. Bennett, T. K. Todorova, E. F. Baxter, D. G. Reid, C. Gervais, B. Bueken, B. Van de Voorde, D. De Vos, D. A. Keen and C. Mellot-Draznieks, *Phys. Chem. Chem. Phys.*, 2016, **18**, 2192–2201.

8 S. Li, S. Yu, S. M. Collins, D. N. Johnstone, C. W. Ashling, A. F. Sapnik, P. A. Chater, D. S. Keeble, L. N. McHugh, P. A. Midgley, D. A. Keen and T. D. Bennett, *Chem. Sci.*, 2020, **11**, 9910–9918.

9 L. Frentzel-Beyme, P. Kolodzeiski, J.-B. Weiß, A. Schneemann and S. Henke, *Nat. Commun.*, 2022, **13**, 7750.